Title

T-Cell-Intrinsic Receptor Interacting Protein 2 Regulates Pathogenic T Helper 17 Cell Differentiation

Journal

Immunity, 49(5)

ISSN

1074-7613

Authors

Shimada, Kenichi
Porritt, Rebecca A
Markman, Janet L
et al.

Publication Date

2018-11-01

DOI

10.1016/j.immuni.2018.08.022

Peer reviewed

HHS Public Access

Author manuscript

Immunity. Author manuscript; available in PMC 2019 November 20.

Published in final edited form as:

Immunity. 2018 November 20; 49(5): 873–885.e7. doi:10.1016/j.immuni.2018.08.022.

T cell intrinsic Receptor Interacting Protein 2 regulates pathogenic T helper-17 cell differentiation

Kenichi Shimada[#1,2,3,7], **Rebecca A. Porritt**[#1], **Janet L. Markman**[1], **Jacqueline Gire O'rourke**[4], **Daiko Wakita**[1], **Magali Noval Rivas**[1,2,3,7], **Chihiro Ogawa**[6], **Lina Kozhaya**[8], **Gislâine A. Martins**[3,6,7], **Derya Unutmaz**[8], **Robert H. Baloh**[4,5], **Timothy R. Crother**[#1,2,3,7], **Shuang Chen**[#1,2,3,7], and **Moshe Arditi**[#1,2,3,7,11,*]

[1]Department of Pediatrics, Division of Infectious Diseases and Immunology, Los Angeles, California 90048, USA.

[2]Department of Biomedical Sciences, Infectious and Immunologic Disease Research Center, Los Angeles, California 90048, USA.

[3]Department of Biomedical Science, Research Division of Immunology, Los Angeles, California 90048, USA.

[4]Board of Governors Regenerative Medicine Institute, Los Angeles, California 90048, USA.

[5]Department of Neurology, Los Angeles, California 90048, USA.

[6]F. Widjaja Foundation Inflammatory Bowel and Immunobiology Research Institute, Cedars-Sinai Medical Center, Los Angeles, California 90048, USA.

[7]David Geffen School of Medicine, University of California, Los Angeles, California 90095, USA,

[8]The Jackson Laboratory for Genomic Medicine, Farmington, Connecticut 06032, USA.

[11]Lead Contact

[#] These authors contributed equally to this work.

SUMMARY

Receptor Interacting Protein 2 (RIP2) plays a role in sensing intracellular pathogens, but its function in T cells is unclear. We show that RIP2 deficiency in $CD4^+$ T cells resulted in chronic and severe interleukin-17A mediated inflammation during *Chlamydia pneumoniae* lung infection, increased T helper-17 (Th17) cell formation in lungs of infected mice, accelerated atherosclerosis, and more severe experimental autoimmune encephalomyelitis. While RIP2 deficiency resulted in

[*]Correspondence: moshe.arditi@cshs.org.

AUTHOR CONTRIBUTIONS

Conceptualization, K.S., T.R.C, S.C., and M.A.; Methodology, K.S., R.A.P.,; Investigation, K.S., R.A.P, J.L.M, J.G.O, D.W., M.N.R., C.O., L.K., S.C., D.U. R.H.B.; Writing, K.S., R.A.P., T.R.C., S.C., and M.A.; Funding Acquisition, M.A., S.C., and T.R.C.; Resources, M.A. and S.C.; Supervision, M.A., K.S., S.C., T.R.C., and G.A.M.

Declaration of Interests: The authors declare no competing interests.

reduced conventional Th17 cell differentiation, it led to significantly enhanced differentiation of pathogenic (p)Th17 cells, which was RORα transcription factor and interleukin-1 dependent, but Nucleotide Oligomerization Domain 1 and 2 independent. Overexpression of RIP2 resulted in suppression of pTh17 cell differentiation, an effect mediated by its CARD domain, and phenocopied by a cell permeable RIP2 CARD peptide. Our data suggest that RIP2 has a T cell intrinsic role in determining the balance between homeostatic and pathogenic Th17 cell responses.

Pathogenic Th17 Cell Differentiation

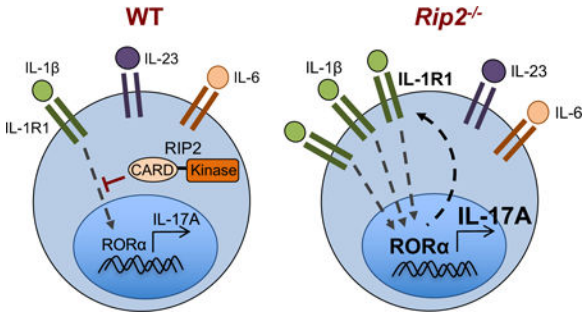

eTOC Blurb

RIP2 is the key adapter molecule for NOD1 and NOD2 mediated intracellular signaling to sense pathogens and cell activation in myeloid cells. Shimada, Porritt and colleagues demonstrate a previously unappreciated role for RIP2 in Th17 cell regulation and differentiation in a T cell intrinsic manner.

Keywords

RIP2, IL-17; Th17; Chlamydia pneumoniae; chronic inflammation; atherosclerosis; RORα

INTRODUCTION

T helper (Th) 17 cells and interleukin-17A (IL-17A) are now recognized as critically important players in various pathologies, both autoimmune and in responses to infections. Indeed, IL-17A plays a major role in colitis, cancer, psoriasis, experimental autoimmune encephalomyelitis (EAE), and numerous infection models (Patel and Kuchroo, 2015). Th17 cells are normally induced by the presence of a combination of cytokines, such as transforming growth factor-β (TGF-β) and IL-6 (Veldhoen et al., 2006). This “conventional” induction of IL-17A normally requires activation of the transcription factors RORγt, IRF4, and BATF among others, which in turn induce the Th17 cell program (Yosef et al., 2013). Alternative induction of Th17 cells using cytokines such as IL-1β, IL-6 and IL-23 result in a more “pathogenic” Th17 (pTh17) cell (Ghoreschi et al., 2010). While the frequency and distribution of these various types of Th17 cells are currently under intense investigation by many laboratories, there is still much to be learned in order to understand the impact of the various Th17 cell programs.

The receptor-interacting protein 2 (RIP2) kinase serves as the signaling adapter protein for the NOD1 and NOD2 intracellular receptors that recognize peptidoglycan, a component of bacterial cell walls, and the muramyl dipeptide structure found in almost all bacteria (Girardin et al., 2003; Ogura et al., 2001). Binding of the receptors by its ligands induces a signaling cascade that will result in NF-κB activation and subsequent downstream cytokine production (Girardin et al., 2003). These pathways are present in many cell types, including myeloid cells and neutrophils. However, the role of RIP2 in T cells has been much less studied and unappreciated. Previous investigations into the role of RIP2 in Th1 cell and Th2 cell differentiation did not report any effect on these pathways (Fairhead et al., 2008; Hall et al., 2008).

In a previous study, we identified RIP2 as a critical signaling molecule in directing immune responses to *Chlamydia pneumoniae* (CP) infection in mice (Shimada et al., 2009). CP, an obligate intracellular bacterium, has been associated with chronic lung diseases, including chronic bronchitis, asthma, chronic obstructive pulmonary disease, and other chronic diseases such as multiple sclerosis, atherosclerosis, and Alzheimer's disease (Shimada et al., 2012). CP clearance is impaired in *Rip2*$^{-/-}$ mice in macrophages, leading to delayed bacterial clearance. We additionally observed a sustained chronic lung inflammation in these mice, despite eventual bacterial clearance, but the mechanisms driving this late inflammation are unknown.

In this study, we first investigated the mechanism driving chronic lung inflammation in *Rip2*$^{-/-}$ mice observed upon CP infection. Restimulation of draining lymph nodes from *Rip2*$^{-/-}$ infected mice showed increased IL-17A and decreased interferon-γ (IFN-γ) production, suggesting a possible mechanism for the chronic lung inflammation. We found that naïve *Rip2*−/− T cells preferentially differentiated towards pTh17 cells in a T cell intrinsic manner and this was IL-1β dependent. In contrast *Rip2*$^{-/-}$ T cells had reduced cTh17 cell differentiation. This altered T cell differentiation was independent of NOD1 and NOD2. Gene expression data revealed that *Rip2*$^{-/-}$ T cells expressed greater amounts of *Rora* and *Il1r1* compared with WT T cells during pathogenic Th17 cell differentiation, but not under conventional (cTh17) cell conditions. RORα is an important transcription factor involved in Th17 cell differentiation (Yang et al., 2008). In line with this, we found that the enhanced pTh17 cell differentiation of *Rip2*$^{-/-}$ cells was RORα dependent. Overexpression of RIP2 in T cells led to a reduction in pTh17 cell differentiation while silencing of *Rip2* resulted in an increase in *Rora* and greater pTh17 cell differentiation. *Il17a*$^{-/-}$*Rip2*$^{-/-}$ mice were completely protected from the chronic lung inflammation found in *Rip2*$^{-/-}$ mice, confirming that excess IL-17A in *Rip2*$^{-/-}$ T cells is driving the late and sustained immune responses and inflammation. We also confirmed these results using a mouse model of atherosclerosis and an experimental EAE model, both in which IL-17A plays a critical role in development of disease (Chen et al., 2010a; Jäger et al., 2009). When *Rag1*$^{-/-}$ mice received *Rip2*$^{-/-}$ T cells, we found a significantly accelerated atherosclerosis, as well as a more severe EAE phenotype. These results highlight a previously unappreciated role for RIP2 in Th17 cell regulation and differentiation in a T cell intrinsic manner.

RESULTS

RIP2 deficiency in T cells increases IL-17A production.

We previously reported that RIP2 deficiency impairs host immune responses against *C. pneumoniae*, resulting in delayed bacterial clearance, increased mortality, and a severe chronic lung inflammation (Shimada et al., 2009). The defective bacterial clearance and increased mortality are rescued by adoptive transfer of WT macrophages. However, we became interested in the development of chronic lung inflammation, despite eventual bacterial clearance. Upon further investigation, we found that lung $CD4^+$ T cells from *Rip2*$^{-/-}$ mice 21 days post infection (p.i.) produced more IL-17A upon restimulation (Figure 1A). Enhanced IL-17A production in *Rip2*$^{-/-}$ mice was largely dependent upon $CD4^+$ T cells as other IL-17A producing cells showed little to no increase in IL-17A production (Figure 1B, Figure S1A). Additionally, there was no observed difference in the numbers of IL-17A producing pulmonary type 3 innate lymphoid cells (ILC3's) between WT and *Rip2*$^{-/-}$ mice 21 days p.i. (Figure S1B). While we did not observe any differences in the number of IL-17A producing cells in the lung between WT and *Rip2*$^{-/-}$ mice at day 0 or 5 days p.i. (Figure S1C), we found an increase in IL-17A and a decrease in IFN-γ production by restimulated mediastinal lymph node (MLN) cells harvested 5 days p.i. (Figure 1C). Furthermore, we observed that MLN cells from infected *Rip2*$^{-/-}$ mice produced more IL-17A and less IFN-γ in a dose dependent manner with specific antigen (UV-killed CP, UVCP) stimulation (Figure 1D). These data strongly suggested that RIP2 deficiency skewed T cells to differentiate towards Th17 cells. To determine whether or not this was a T cell intrinsic effect, we isolated $CD4^+$ T cells from spleens of infected WT and *Rip2*$^{-/-}$ mice, which were then co-cultured with UVCP-preloaded WT bone marrow dendritic cells (BMDC). *Rip2*$^{-/-}$ $CD4^+$ T cells produced significantly more IL-17A and less IFN-γ than WT (Figure 1E). Since UVCP contains LPS, we also stimulated the T cells with LPS as a control, but did not observe any significant effect on IL-17A production between WT and *Rip2*$^{-/-}$ (Figure 1E). These data suggested that *Rip2*$^{-/-}$ T cells, but not antigen-presenting cells contributed to the observed increase in IL-17A production during restimulation.

We next wanted to determine if naive *Rip2*$^{-/-}$ $CD4^+$ T cells intrinsically had the capacity to differentiate into Th17 cells *in vivo*. We adoptively transferred naïve WT or *Rip2*$^{-/-}$ $CD4^+$ T cells into *Rag1*$^{-/-}$ mice to examine Th17 cell differentiation during CP infection. While there was no significant difference in the bacterial burden (Day 5) among these mice (Figure 1F), *Rag1*$^{-/-}$ mice adoptively transferred with naive *Rip2*$^{-/-}$ $CD4^+$ T cells produced significantly more IL-17A and less IFN-γ than WT (Figure 1G and H). Taken together, our data demonstrate that RIP2 deficiency in $CD4^+$ T cells leads to enhanced Th17 cell differentiation and suggest that RIP2 plays a T cell intrinsic role in down regulating Th17 cell differentiation.

RIP2 deficient naïve $CD4^+$ T cells preferentially differentiate towards pathogenic Th17 cells *in vitro*.

During CP infection, RIP2 deficiency led to increased IL-17A production by both MLN cells and $CD4^+$ splenic T cells after restimulation and did not require *Rip2*$^{-/-}$ antigen presenting cells (APCs) during the restimulation. However, it was unclear if the preferential

Th17 cell differentiation was the result of pre-programming of T cells during CP infection or preferential differentiation during restimulation. We isolated naïve $CD4^+$ T cells and stimulated them under cTh17 cell (IL-6 and TGF-β) or pTh17 cell (IL-1β, IL-6, and IL-23) conditions to address whether RIP2 deficiency altered differentiation of naïve $CD4^+$ T cells. We observed that naïve $CD4^+$ T cells that lacked *Rip2* had reduced IL-17A production under cTh17 cell conditions yet enhanced IL-17A production under pTh17 cell conditions (Figure 2A–C) (Ghoreschi et al., 2010). The opposing role of RIP2 in cTh17 cell and pTh17 cell conditions was evident by both the percent of cells that produced IL-17A and the concentration of IL-17A in the culture supernatant (Figure 2A–C). To investigate whether RIP2 was acting downstream of NOD1 and NOD2 as per the canonical RIP2 pathway we performed *in vitro* Th17 cell differentiation in $CD4^+$ naïve T cells from WT, $Nod2^{-/-}$ and $Nod1^{-/-}Nod2^{-/-}$ mice. Our data revealed no difference in cTh17 cell and pTh17 cell differentiation indicating that the T cell intrinsic effect of RIP2 was independent of NOD1 and NOD2 signaling (Figure S2). To further investigate the T cell intrinsic nature of the observed Th17 cell differentiation in $Rip2^{-/-}$ T cells, we mixed and matched naive WT and $Rip2^{-/-}$ T cells with WT or $Rip2^{-/-}$ antigen presenting cells (APCs) under pathogenic Th17 cell differentiation conditions and found that the increased IL-17A production was unrelated to the genotype of the APCs, instead it was only the T cell genotype that mattered (Figure 2D). We also investigated whether RIP2 deficiency altered T cell proliferation and indeed found that $CD4^+$ T cells lacking *Rip2* proliferated more than WT cells under pTh17 cell conditions (Figure 2E). Given the relationship between regulatory T (Treg) cells and Th17 cells, we investigated whether RIP2 deficiency affected Treg cell suppression activity and differentiation. Importantly, RIP2 deficiency did not alter Treg cell suppression function (Figure 2F) or the differentiation of Treg cells *in vitro* (Figure 2G). In addition to IL-17A, Th17 cells can also produce IL-17F, and the IL-17A and F heterodimer (Wright et al., 2007). However, while we did not observe an increase in IL-17F production in $Rip2^{-/-}$ T cells, there was an increase in the amount of heterodimer produced (Figure 2H).

Taken together, both our *in vitro* and *in vivo* data demonstrate that RIP2 deficiency in $CD4^+$ T cells leads to enhanced pTh17 cell differentiation and suggest that RIP2 plays a T cell-intrinsic role in down regulating pathogenic Th17 cells. Conversely our *in vitro* data suggest that RIP2 deficiency has opposing effects on cTh17 cell differentiation, suggesting RIP2 may act as a balancing factor between the homeostatic and pathogenic roles of Th17 cells.

C. pneumoniae induced chronic inflammation in $Rip2^{-/-}$ mice is driven by IL-17A.

$Rip2^{-/-}$ mice develop a severe chronic lung inflammation during CP infection (Shimada et al., 2009) that is accompanied with increased IL-17A production (Figure 1). However, the role of IL-17A in CP pathogenesis is not fully understood. A previous study did find a slight increase in CP IFUs early (day 4) during infection after administering IL-17A neutralizing antibodies (Mosolygó et al., 2013), however, in that study it was not clear how efficient IL-17A neutralization was. In order to better understand if IL-17A is required in host immune responses for CP and CP-induced pathology, we examined the role of IL-17A during CP lung infection using $Il17a^{-/-}$ mice. We did not find delayed bacterial clearance and there were no changes in lung bacterial burden 5 or 14 days p.i. (Figure 3A). Despite the lack of difference in bacterial burden found between WT and $Il17a^{-/-}$ mice, there was a

reduction in inflammation in the lungs of *Il17a*$^{-/-}$ mice 14 days after CP infection (Figure 3B and 3C) as well as a reduction in the total number of cells in the lung 14 days p.i. (Figure 3D). Numerous studies have found that IL-17A plays a role in neutrophil recruitment during infection (Huang et al., 2004; Kelly et al., 2005; Ye et al., 2001). While we did not observe any defect in early (day 5) neutrophil recruitment in *Il17a*$^{-/-}$ mice during CP infection, we found that neutrophil numbers were significantly reduced 14 days p.i. (Figure 3E and S3) despite a similar bacterial burden (Figure 3A). CD4^{+} T cell recruitment was also decreased in *Il17a*$^{-/-}$ mice 14 days p.i. (Figure 3F and 3G). These data suggest that IL-17A is dispensable for host defenses against CP infection but instead mediates the later stages of CP-induced sustained lung inflammation.

Our data suggest that RIP2 deficiency in CD4^{+} T cells enhances Th17 cell differentiation. Therefore, we hypothesized that RIP2 deficiency exacerbates IL-17A-mediated chronic inflammation in *Rip2*$^{-/-}$ mice and is likely responsible for the severe chronic lung inflammation that we previously reported (Shimada et al., 2009). To address this, we generated *Il17a*$^{-/-}$*Rip2*$^{-/-}$ mice and infected them with CP, followed by euthanasia 35 days p.i.. While *Rip2*$^{-/-}$ mice developed severe lung inflammation 35 days p.i. as expected, *Il17a*$^{-/-}$*Rip2*$^{-/-}$ mice did not develop measurable inflammation (Figure 3H and 3I) underscoring the role of IL-17A in RIP2 deficiency mediated chronic lung inflammation. Since we had previously observed that CP was cleared from the lung in *Rip2*$^{-/-}$ mice 35 days p.i. (Shimada et al., 2009), we assessed bacterial burden 5 days p.i. in *Il17a*$^{-/-}$*Rip2*$^{-/-}$ mice. Importantly, *Il17a*$^{-/-}$*Rip2*$^{-/-}$ mice had similar delayed bacterial clearance as *Rip2*$^{-/-}$ mice, again indicating that IL-17A does not play a substantial role in controlling CP bacterial burden (Figure 3J). These observations clearly suggest that IL-17A is responsible for the pathogenesis of chronic lung inflammation we have observed in the *Rip2*−/− mice during CP infection.

RIP2 deficiency enhances IL-17A dependent atherogenesis.

While our data show that IL-17A plays a critical role in CP infection induced chronic lung inflammation in *Rip2*$^{-/-}$ mice, we sought to investigate whether RIP2 deficiency exacerbated another disease pathology associated with IL-17A, atherosclerosis (Butcher et al., 2012; Chen et al., 2010b; Gao et al., 2012). In an initial study we transferred WT, *Rip2*$^{-/-}$, o*r Il17a*$^{-/-}$*Rip2*$^{-/-}$ bone marrow into irradiated *Ldlr*$^{-/-}$ mice. After bone marrow reconstitution (8 weeks), the chimeric mice were fed a HFD for 12 weeks. The *Rip2*$^{-/-}$ chimeric mice exhibited a significant increase in lesion size in the aortic sinus and aorta en face (Figure S4A–D), despite a similar serum cholesterol concentration (data not shown). This increase was abrogated in the *Il17a*$^{-/-}$*Rip2*$^{-/-}$ chimeric mice.

However, this experiment did not rule out the possibility that RIP2 played a role in immune cells other than T cells. We therefore performed an adoptive transfer of WT, *Rip2*$^{-/-}$, o*r Il17a*$^{-/-}$*Rip2*$^{-/-}$ naive CD4^{+} T cells into *Rag1*$^{-/-}$ mice. In order to induce hyperlipidemia, the mice were administered with AAV-PCSK9, which contains a gain of function mutation leading to enhanced degradation of the LDL receptor (Roche-Molina et al., 2015). After 12 weeks HFD feeding, *Rag1*$^{-/-}$ mice that received *Rip2*$^{-/-}$ T cells had larger lesions in the aortic sinus and aorta en face (Figure 4A–E) despite a similar serum cholesterol

concentration (data not shown). This increase was completely abrogated when *Il17a*$^{-/-}$*Rip2*$^{-/-}$ T cells were transferred instead. Additionally, there was significantly more IL-17A in the serum of mice that received *Rip2*$^{-/-}$ T cells (Figure 4F), as well as an increased number of IL-17A producing CD4^{+} T cells in the spleen and PBMCs (Figure 4G and 4H). Taken together, these data indicate that RIP2 deficiency in T cells leads to accelerated atherogenesis via IL-17A production.

RIP2 deficiency in T cells enhances EAE severity and mortality

While IL-17A clearly plays a role in atherogenesis, atherosclerosis is a multifactorial inflammatory disease with many contributing factors. We therefore assessed whether the loss of *Rip2* in T cells would exacerbate another well studied disease model, EAE, which has a primary contribution from pTh17 cells (Ghoreschi et al., 2010). In order to investigate the T cell intrinsic effect of RIP2 deficiency, we adoptively transferred WT and *Rip2*$^{-/-}$ CD4^{+} T cells into *Rag1*$^{-/-}$ mice and then immunized them with the MOG antigen to induce EAE. While adoptive transfer of WT CD4^{+} T cells led to a moderate disease severity, mice that received *Rip2*$^{-/-}$ CD4^{+} T cells displayed a significantly ($p < 0.001$) more severe disease phenotype (Figure 5A) which led to a significant ($p < 0.05$) increase in mortality (Figure 5B). Thus, RIP2 deficiency in CD4^{+} T cells alone leads to a significantly more pathogenic EAE phenotype, confirming the T cell intrinsic role of Rip2 in pathogenic Th17 cell development.

RORα and IL-1β mediate the enhanced pathogenic Th17 cell differentiation of RIP2 deficient T cells.

Rip2$^{-/-}$ naïve CD4^{+} T cells are prone to differentiate towards Th17 cells under pathogenic Th17 cell differentiation conditions (Figure 2A–B). Consistent with this observation, we found that *Il17a* was indeed upregulated in these cells (Figure 6A). However, we did not observe any difference in *Rorc* transcript expression between WT and *Rip2*$^{-/-}$ pTh17 cells (Figure 6B). Instead, we observed increased expression of *Rora* in *Rip2*$^{-/-}$ T cells (Figure 6C). In an effort to confirm our data, we silenced *Rip2* expression using shRNA in naïve CD4^{+} T cells. T cells silenced for *Rip2* expression and differentiated under pathogenic Th17 cell conditions produced greater amounts of IL-17A and expressed significantly more *Rora* (Figure 6D and 6E). RORα was recently described to be expressed in Th17 cells and act in synergy with RORγt to promote Th17 cell differentiation (Yang et al., 2008). In addition to *Rora* mRNA expression, *Rip2*$^{-/-}$ CD4^{+} T cells displayed more RORα protein expression than WT (Figure 6F). Importantly, RORα protein expression correlated with IL-17A production (Figure 6G–I). To corroborate these associations, we identified two RORα binding sites (CNS1, CNS2) in the *Il17a* locus and performed a ChIP assay using anti-RORα antibody. Under pathogenic Th17 cell skewing conditions, we found that RORα bound to CNS 1 and 2 four to eight-fold higher respectively in *Rip2*$^{-/-}$ CD4^{+} T cells compared with WT CD4^{+} T cells (Figure 6J). To determine the contribution of RORα to RIP2 mediated regulation of IL-17A production, we performed siRNA mediated silencing of *Rora* in *Rip2*$^{-/-}$ CD4^{+} naïve T cells differentiated under pTh17 cell conditions. We found reduced IL-17A production in *Rip2*$^{-/-}$ cells treated with si*Rora* compared with controls (Figure 6K). To confirm this, we performed another experiment in which we used siRNA to silence *Rip2* and *Rora*, alone or in combination, in CD4^{+} naïve T cells under pTh17 cell

differentiation conditions. Indeed, we found that siRNA mediated silencing of *Rip2* led to enhanced IL-17A production and importantly this was abrogated with the additional silencing of *Rora* (Figure 6L). Next, we assessed transcript expression of known factors involved in pTh17 cell differentiation. While we found no significant differences in *Tbx21*, *Ifng*, *Il23r*, *Csf2*, and *Il10* between WT and *Rip2*$^{-/-}$ T cells (Figure 6M), we observed a significant increase in *Il1r1* in *Rip2*$^{-/-}$ T cells (Figure 6M). To determine if RORα was responsible for the enhanced expression of *Il1r1*, we performed siRNA mediated silencing of *Rora* in *Rip2*$^{-/-}$ T cells differentiated under pTh17 cell conditions. We found that there was a substantial reduction in *Il1r1* with *Rora* silencing (Figure 6N), indicating that the enhanced expression of RORα in *Rip2*$^{-/-}$ T cells is responsible for increased IL-1 receptor 1 (IL-1R1) expression. These results, which are consistent with published studies showing RORα regulation of IL-1R1, led us to further investigate the contribution of IL-1β signaling to the enhanced differentiation of *Rip2*$^{-/-}$ pTh17 cells (Chung et al., 2009). We performed differentiation of WT or *Rip2*$^{-/-}$ naïve CD4^{+} T cells under normal pTh17 cell conditions or without IL-1β. IL-17A expression and *Rora* were reduced in both WT and *Rip2*$^{-/-}$ cells in the absence of IL-1β. Importantly, our results show the differential production of IL-17A and *Rora* expression by *Rip2*$^{-/-}$ cells under pTh17 cell conditions was completely abrogated in the absence of IL-1β (Figure 6O and 6P). The addition of Anakinra, an IL-1R1 antagonist, during pTh17 cell differentiation also abrogated the difference in IL-17A expression (Figure S5). These data indicate that IL-1β signaling is necessary for enhanced *Rora* mediated pTh17 cell differentiation of *Rip2*$^{-/-}$ CD4^{+} T cells. Taken together, our data suggests that RIP2 may function to suppress a RORα – IL-1β signaling positive feedback loop during pTh17 cell differentiation. Of note, while we observed that *Rorc* was not changed in pTh17 cells (Figure 6B), *Rorc* was significantly reduced in *Rip2*$^{-/-}$ CD4^{+} T cells under cTh17 cell differentiation conditions (Figure S6A), with *Rora* displaying a reducing trend (Figure S6B). These data corroborate the reduction in cTh17 cell differentiation observed in *Rip2*$^{-/-}$ T cells (Figure 2A and B). Additionally, we observed that under cTh17 cell conditions, *Rip2*$^{-/-}$ T cells also displayed a reduction in *Tbx21*, *Ifng*, *Il23r*, *Il1r1*, and *Csf2*, with no observed differences in *Il10* (Figure S6C–H). Overall our data suggest that the mechanism by which RIP2 deficiency leads to enhanced pathogenic Th17 cell differentiation is through RORα, but not RORγt, and that loss of RIP2 expression may conversely lead to a reduction in cTh17 cell formation.

We next sought to investigate if RIP2 also played a role in human Th17 cell regulation. We isolated human memory (CD4^{+}CD45RO+CCR6^{+}) T cells and silenced *Rip2* with shRNA. *Rip2* silencing resulted in increased RORα and IL-17A production (Figure S7A and S7B). Thus, it is likely that RIP2 also plays a similar role in human T cell biology.

RIP2 CARD domain suppresses pathogenic Th17 cell differentiation and *Rora* expression.

Given that the lack of RIP2 leads to increased RORα, we hypothesized that RIP2 itself leads to pTh17 cell suppression and might be regulated during Th17 cell differentiation. We determined the expression of *Rip2* mRNA under Th17 cell differentiation and found that *Rip2* mRNA is significantly downregulated during pTh17 cell differentiation compared to a T cell stimulatory condition (Figure 7A). We next isolated IL-17A producing CD4^{+} T cells from the lungs 21 days after CP infection and found that lung IL-17A producing T cells had

significantly less *Rip2* than IFN-γ producing T cells (Figure 7B). These data suggested an inverse relationship between *Rip2* and pTh17 cells. Analysis of the human and mouse *Rip2* locus identifies putative RORα binding sites, suggesting that downregulation of *Rip2* in pTh17 cells may be directly mediated by RORα (Figure 7A). To investigate how RIP2 may be acting to regulate pTh17 cell differentiation we investigated the contribution of the kinase activity of RIP2 to its function. We treated $CD4^+$ T cells undergoing pTh17 cell differentiation with two different RIP2 kinase inhibitors. This resulted in no difference (GSK583) or a small suppression (OD36) of IL-17A production indicating that the kinase domain is not required for RIP2 deficiency enhanced Th17 cell differentiation (Figure 6C). To determine the domains of RIP2 required for its function, we performed overexpression of RIP2, RIP2 lacking its kinase activity (RIP2K47A) or RIP2 lacking its CARD domain (RIP2ΔCARD). While overexpression of RIP2 in naive $CD4^+$ T cells led to a decrease in IL-17A production under pTh17 cell differentiation conditions (Figure 7D), overexpression of RIP2K47A only had a moderate effect on preventing pTh17 cell differentiation (Figure 7D). In contrast, overexpression of RIP2ΔCARD was unable to inhibit pTh17 cell differentiation (Figure 7D), suggesting that the CARD domain was required for RIP2 to exert its effect. Consistent with our model, overexpression of just the RIP2 CARD domain (RCD) led to a significant decrease in IL-17A production under pTh17 cell conditions (Figure 7E). Furthermore, treatment with a cell permeable (Lim et al., 2015) RCD led to a dose dependent decrease in pTh17 cell differentiation and a reduction in *Rora* expression (Figure 7F and G). These data therefore indicate that it is the CARD domain of RIP2, not its kinase domain, that mediates regulation of pTh17 cell differentiation. Overall, our data strongly suggest that RIP2 plays a T cell intrinsic negative feedback role during pTh17 cell differentiation.

DISCUSSION

The serine and threonine kinase RIP2 is the key adapter molecule for NOD1 and NOD2 mediated intracellular signaling to sense pathogens and cell activation in innate immune cells (Ogura et al., 2001). In this study, we discovered that in addition to its innate immune signaling properties in myeloid cells, RIP2 also functions as a T cell intrinsic repressor of pTh17 cell differentiation, and in its absence, T cells are preferentially polarized towards Th17 cells under pathogenic conditions. In contrast, the absence of *Rip2* resulted in reduced Th17 cell polarization under conventional conditions. The consequences of this regulation are that in $Rip2^{-/-}$ mice, the Th17 cell population may become exaggerated and lead to enhanced inflammation and a more pathogenic chronic inflammatory state. We observed that both *in vitro* and *in vivo* RIP2 deficiency leads to enhanced pTh17 cell differentiation that was directly responsible for exacerbated chronic lung inflammation, enhanced atherosclerosis, and more severe EAE in $Rip2^{-/-}$ mice. Initial investigations into the role of Rip2 in T cells reported defects in Th1 cell differentiation and TCR signaling as a result of RIP2 deficiency (Chin et al., 2002; Kobayashi et al., 2002; Ruefli-Brasse et al., 2004). However, later studies disputed these findings, thus making the role of RIP2 in T cells controversial (Fairhead et al., 2008; Hall et al., 2008; Nembrini et al., 2008).

Levin et al. also reported that RIP2 deficiency led to increased atherosclerosis using BMT into $Apob^{100/100}$ $Ldlr^{-/-}$ mice (Levin et al., 2011). They showed that $Rip2^{-/-}$ macrophages

have upregulated TLR4 expression, which resulted in TLR4-dependent increase in foam cell formation. However, it is unclear whether this upregulated TLR4 expression was involved in the mechanism of increased atherogenesis in *Rip2*$^{-/-}$ mice. We report that in the presence of NODs signaling during CP infection, *Rip2*$^{-/-}$ mice had enhanced atherogenic lesions, even though *Rip2*$^{-/-}$ macrophages showed defective CP-induced foam cell formation, indicating that RIP2 deficiency in T cells rather than macrophages is responsible for the increased atherogenesis we observed. Indeed, we did not observe any increase of foam cell formation in *Rip2*$^{-/-}$ macrophages in the presence of TLR4 agonist (data not shown). Further supporting this argument, a study by Park et al did not observe any increased proinflammatory cytokine production in response to LPS in *Rip2*$^{-/-}$ macrophages compared with WT (Park et al., 2007). In our experiments with T cell adoptive transfer model of atherosclerosis, we still observed accelerated lesion development with *Rip2*$^{-/-}$ T cells, highlighting the intrinsic effect to the T cell. Finally, we found that the acceleration of atherogenesis in *Rip2*$^{-/-}$ mice was completely abrogated with *Il17a*$^{-/-}$*Rip2*$^{-/-}$ T cells, indicating the critical role of IL-17A in the acceleration of atherosclerosis in *Rip2*$^{-/-}$ mice.

In a recent study, RIP2 deficiency was found to have a suppressive effect on the EAE model of multiple sclerosis (Shaw et al., 2011). EAE progression has been linked to IL-17 as the development of EAE was markedly suppressed in *Il17*$^{-/-}$ mice (Komiyama et al., 2006). While the data from Shaw et al at first may seem contradictory to our findings, there is a technical pitfall in that EAE model requires Complete Freund's Adjuvant, which includes Mycobacterial peptidoglycan signaling through NOD1, NOD2 and RIP2. Thus, the results from this earlier study can be interpreted that NOD1, NOD2 and RIP2 deficient mice lack proper innate immune signaling for MOG immunization, hence the lack of or diminished EAE development, as mentioned by the authors themselves (Shaw et al., 2011). Indeed, using a *Rip2*$^{-/-}$ CD4^{+} T cell specific model of EAE, we report a profound increase in disease severity and mortality compared with WT CD4^{+} T cells, highlighting the pathogenic nature of *Rip2*$^{-/-}$ T cells.

In addition to CD4^{+} T cells, other IL-17A-producing cell population exists; γδ T cells, CD3^{+} iNK cells, lymphoid-tissue inducer (LTi)-like cells, and NK cells are important innate IL-17A-producing cells during autoimmune inflammation and infectious diseases (Miossec and Kolls, 2012). Innate IL-17A-producing cells can induce epithelial cell secretion of granulopoietic factors such as G-CSF and CCL20, which can lead to neutrophil infiltration, which is crucial for effective and rapid control of pathogens such as *Klebsiella pneumoniae*, *Staphylococcus aureus*, and *Candida albicans* (Aujla et al., 2008; Huang et al., 2004; Ishigame et al., 2009). In our study, IL-17A was involved in the persistence and late recruitment of neutrophils during *C. pneumonia*-induced chronic lung infection, possibly through Th17 cell derived IL-17A leading to G-CSF production from stromal cells. IL-17A did not pay a role in bacterial clearance of CP infection, indicating that IL-17A is not involved in the initial host defenses against CP, which is an intracellular pathogen. On the other hand, in *Escherichia coli* acute pulmonary infection, *Rip2*$^{-/-}$ mice had reduced IL-17A production from NK cells and γδ T cells (Balamayooran et al., 2011), indicating that RIP2 deficient cellular responses are distinguishable between acute and chronic infections.

Previous publications have found a link between gut microbiota and Th17 cell populations in mice (Ivanov et al., 2008). However, our *in vitro* data using naïve $CD4^+$ T cells clearly revealed an intrinsic enhancement of Th17 cell differentiation, and more importantly, the adoptive transfer of naïve $CD4^+$ WT and *Rip2*$^{-/-}$ T cells into *Rag1*$^{-/-}$ mice provides identical microbiota host milieus, suggesting it is the *Rip2*$^{-/-}$ T cell itself, and not any other external factor that drives the Th17 cell enhancement.

Our data demonstrate that this T cell specific role of RIP2 in Th17 cell differentiation is independent of the NOD1 and NOD2 signaling pathway, suggesting RIP2 may be activated via an alternative method in T cells. Several publications implicate that NOD1, NOD2 and RIP2 are involved in other pathways besides sensing bacterial peptidoglycan both *in vitro* and *in vivo*. *Nod1*$^{-/-}$*Nod2*$^{-/-}$ BMDM respond to endoplasmic reticulum stress inducers differently (Keestra-Gounder et al., 2016), and NOD2 interacts with the small GTPase RAC1 under actin disruption by cytochalasin D (Legrand-Poels et al., 2007). *Nod1*$^{-/-}$, *Nod2*$^{-/-}$ or *Rip2*$^{-/-}$ mice have shown various phenotypes in non-bacterial infection studies, such as atherosclerosis (Levin et al., 2011), myocardial infarction (Li et al., 2015), influenza virus infection (Lupfer et al., 2013). Our data indicate some key mechanisms by which RIP2 mediates signaling in T cells. RORα, a Th17 cell transcription factor, was upregulated in *Rip2*$^{-/-}$ pTh17 cells compared with WT cells. RORα was recently shown to be important in Th17 cell differentiation and to work in synergy with the transcription factor RORγt (Yang et al., 2008). While we did not observe any difference in *Rorc* expression, we show that RORα is responsible for the enhanced Th17 cell differentiation and IL-17A production in *Rip2*$^{-/-}$ cells under pathogenic conditions. Our data also indicate that the increased expression of IL-1R1 that we observed in *Rip2*$^{-/-}$ $CD4^+$ T cells under pathogenic conditions was dependent on RORα upregulation, consistent with a prior study that reported RORα regulates IL-1R1 expression (Yang et al., 2008). Furthermore, our data also suggest that IL-1β signaling is required for enhanced *Rora* expression and pTh17 cell differentiation in *Rip2*$^{-/-}$ $CD4^+$ T cells. Taken together our findings indicate that RIP2 may function to suppress the RORα - IL-1β signaling positive feedback loop during pTh17 cell differentiation. IL-1β is generally considered to play a driving role in pathogenic Th17 cell development (Ghoreschi et al., 2010). In two of our *in vivo* models, CP lung infection and atherosclerosis, IL-1β is known to be critically required for host immune responses or contribute to the pathology, respectively (Duewell et al., 2010; Shimada et al., 2011).

Additionally, we observed that under pTh17 cell conditions, $CD4^+$ WT T cells down-regulated *Rip2* mRNA. The *Rip2* locus contains putative RORα binding sites in both human (chr8: 90773142–90773155 and chr8: 90774710–90774723) and mouse (chr4: 16085940–16085952 and chr4: 16087688–16087700), suggesting that RIP2 expression may be regulated by RORα as an intrinsic negative feedback during Th17 cell differentiation.

It remains unclear how RORα is being upregulated in *Rip2*$^{-/-}$ T cells. Although RIP2 possesses serine and threonine kinase activity, the direct interaction of RIP2 and RORα is unlikely due to different subcellular compartmentalization. Indeed, overexpression of RIP2 lacking kinase activity did not significantly affect the inhibition of pTh17 cell differentiation. However, overexpression of RIP2 lacking the CARD domain lost its inhibitory activity for pTh17 cell differentiation, suggestion that the CARD domain was

critical for this function. Indeed, the CARD domain alone was sufficient to inhibit *Rora* expression and pTh17 cell differentiation. Thus, it is likely that RIP2 mediates inhibition of *Rora* through its CARD domain, although it is not clear yet how RIP2 or RCD physically interact with the binding partner(s). Our results identify a pathway that is a prime candidate for targeting therapeutically as it potentially selectively targets pTh17 cells, not homeostatic cTh17 cells. It is also possible that the cell permeable RCD peptide could, in addition to reducing pTh17 cell development, might also boost cTh17 cells, which are beneficial and important for homeostasis (Stockinger and Omenetti, 2017). Therapeutic use of cell permeable RCD may prove effective in the treatment of IL-17A mediated inflammatory diseases while reducing unwanted side effects such as those observed in current anti-IL17A treatments, which arise by loss of homeostatic IL-17 functions.

In addition to αβ $CD4^+$ T cells, γδ T cells, which have high responsiveness to IL-1R1, can produce large quantities of IL-17A in response to IL-1β, and generally as an early response to infection. However, in our experimental CP infection model we did not observe an increase in γδ T cell IL-17A production. While we have not directly examined IL-1R1 expression on *Rip2*$^{-/-}$ γδ T cells, one possible explanation for this observation may be that the development and effector fate mapping of γδ T cells mainly takes place in the thymus and not during cytokine differentiation. Furthermore, a recent study has shown that while RORγt was required for the development of IL-17 producing γδ T cell subsets, RORα was dispensable for normal γδ T cell function (Barros-Martins et al., 2016). Nevertheless, since we have not tested these cells directly, the role RIP2 may play in γδ T cell function will need to be determined in future studies.

The involvement of RIP2 in Th17 cell differentiation in a T cell intrinsic manner provides an important mechanism by which human chronic inflammatory diseases might be mediated. Additionally, the clear association of *Rip2* polymorphisms in various human diseases begs further investigations into the mechanism of RIP2 Th17 cell regulation, thus identifying individuals who might be a greater risk for various chronic inflammatory diseases where increased IL-17A plays a detrimental role, such as chronic lung diseases, atherosclerosis, Crohn's Disease, multiple sclerosis, and other chronic inflammatory diseases.

STAR METHODS

CONTACT FOR REAGENT AND RESOURCE SHARING

Further information and requests for resources and reagents should be directed to and will be fulfilled by the Lead Contact, Moshe Arditi (Moshe.Arditi@cshs.org).

EXPERIMENTAL MODEL AND SUBJECT DETAILS

Experimental Animals—C57BL/6 (B6), *Nod2*$^{-/-}$ B6, *Ldlr*$^{-/-}$ B6 and *Rag1*$^{-/-}$ B6 mice were purchased from Jackson laboratories. *Il17a*$^{-/-}$ B6 mice were kindly provided by Dr. Yoichiro Iwakura (Univ. Tokyo, Tokyo), *Rip2*$^{-/-}$ B6 mice were kindly provided by Dr. Genhong Cheng (Univ. California Los Angeles, Los Angeles, CA). *Nod1*$^{-/-}$*Nod2*$^{-/-}$ B6 mice were kindly provided by Dr. Andreas J. Baumler (Univ. California Davis, Davis, CA). *Ifng*$^{\text{Thy1.1}}$*Il17a*$^{\text{EGFP}}$ reporter B6 mice were kindly provided by Dr. Masayuki Fukata

(Cedars-Sinai Medical Center, Los Angeles, CA). We have crossed for at least 8 generations and established *Rip2*$^{-/-}$*Il17a*$^{-/-}$ mice. Unless otherwise stated, 6–10 weeks old male and female mice were used. Mice were sex and age matched for individual experiments. Mice were housed under pathogen-free conditions at Cedars-Sinai Medical Center. The mice were housed in a 12-hour light: dark cycle and given ad-libitum access to food and water for the duration of the study. All animal experiments were performed under protocols that had been approved by the Institutional Animal Care and Use Committee at our facility.

Cell Lines—HEp2 cells were cultured in RPMI supplemented with 10% FBS. GP2–293 cells were cultured in DMEM supplemented with 10% FBS. Cell culture was performed at 37 °C in 5% CO_2 unless otherwise specified.

Murine Primary Cells—CD4$^+$ naïve T cells were isolated from 6–10-week-old male and female mice and differentiated to T-helper cell subsets as described in *CD4$^+$ T cell Differentiation and Treatment* below. Mice were sex and age matched for individual experiments. For generation of Bone Marrow Dendritic Cells (BMDC's); bone marrow was isolated from 6–10-week-old male and female mice and differentiated as described in *Generation of Bone Marrow Dendritic Cells (BMDC)* below. Isolation and culture of lymphocytes harvested from *in vivo* animal disease models are described for each model below. Cell culture was performed at 37 ° C in 5% CO_2.

Human Samples—Blood samples were obtained from anonymous consenting healthy donors as buffy coats (New York Blood Center). CD4$^+$ T cell isolation and culture are described in *shRNA mediated silencing of RIP2 in Human CD4$^+$ T cells*.

METHOD DETAILS

C. pneumoniae* Infection Model and Analysis—C. pneumoniae* CM-1 (ATCC, Manassa, VA) was propagated in HEp-2 cells as previously described (Shimada et al., 2009). Age and sex matched (6–8-week-old male or female) mice were intratracheally infected with *C. pneumoniae* by inoculating 100 μl of PBS containing 1×10^6 IFU of the microorganism. For *Rag1*$^{-/-}$ studies; WT or *Rip2*$^{-/-}$ splenic naive CD4$^+$ T cells (CD4$^+$CD44$^-$CD62L$^+$CD25$^-$) were isolated by flow sorting with BD FACS Aria II and 3×10^6 cells were adoptively transferred i.v. to *Rag1*$^{-/-}$ mice 1 day prior to inoculation. Mice were euthanized 5, 14, 21 or 35 days post infection for analysis, as indicated. To quantify *C. pneumoniae* progeny in the lung, the inferior and post-caval lobes were homogenized with 1ml of sucrose-phosphate-glutamate medium. HEp2 cells were inoculated with lung specimens or cell lysates and bacterial counts determined with the as previously described using the Pathfinder Chlamydia Culture Kit (Shimada et al., 2009). For analysis of lung pathology, the left lung was fixed in formalin buffer, paraffin-embedded, and hematoxylin and eosin (H&E)-stained sections were scored by a trained pathologist blinded to the genotypes as previously described (Shimada et al., 2009). For analysis of lung lymphocyte populations; lymphocytes were isolated by digesting the superior and middle lobes at 37°C for 20 minutes in HANKS buffer containing 40 U/ml Liberase and 50 U/ml DNase1 then filtered through a 70 μm cell strainer followed by RBC lysis. For assessment of lung lymphocyte populations, flow cytometry was performed as described in *Flow Cytometry* below. For

assessment of MLN cell cytokine expression at 21 days post infection, 2×10^5 lymph node cells were stimulated with plate bound anti-CD3 and anti-CD28, UV-killed *C. pneumoniae* (MOI 5, unless otherwise indicated) or LPS (100 ng/ml). The supernatants were collected on day 3 post stimulation and production of IFN-γ and IL-17A were measured by ELISA. For analysis of cytokine production by splenic $CD4^+$ T cells, spleens were harvested at day 5 post infection and $CD4^+$ T cells were isolated with a mouse $CD4^+$ T cell isolation kit (Miltenyi Biotec). $CD4^+$ T cells were co-cultured with BMDCs pre-loaded with UVCP (MOI 5) or stimulated with LPS (100 ng/ml). Supernatants were collected on day 3 of culture and production of IFN-γ and IL-17A were measured by ELISA. Cell culture was performed at 37 °C in 5% CO_2.

Atherosclerosis Model and Analysis—Age matched male *Rag1*$^{-/-}$ mice were adoptively transferred with WT or *Rip2*$^{-/-}$ $CD4^+CD44^+CD62L^+CD25^-$ T cells (3×10^6) i.v. and one week later were injected i.v. with AAVPCSK9 (1×10^{11}). Mice were fed for 12 weeks on a high (0.15%)-cholesterol diet (High Fat Diet, HFD) (TD88137, Harlan Teklad, Madison, WI). For bone marrow transplantation; *Ldlr*$^{-/-}$ mice were exposed to sublethal irradiation and transplanted with WT, *Rip2*$^{-/-}$ or *Rip2*$^{-/-}$*Il17a*$^{-/-}$ BM (5×10^6) i.v. 6 weeks after transplant, mice were fed a HFD for 12 weeks then euthanized for analysis. The aortas were dissected and the adherent (adventitial) fat was gently removed. Whole aortas were opened longitudinally from the aortic arch to the iliac bifurcation, mounted *en face*, and stained for lipids with Oil Red O. Hearts were embedded in OCT (Tissue-Tek; Sakura, Torrance, CA) and serial 7 μm–thick cryosections from the aortic sinus were mounted and stained with Oil Red O and hematoxylin. Image analysis was performed by a trained observer blinded to the genotype of the mice. Representative images were obtained and lesion areas were quantified with Image analysis software using a BZ-X710 microscope (Keyence, Itasca, IL). The lesion area and lipid-stained area were measured as previously described (Tumurkhuu et al., 2016). Blood was collected by retro-orbital bleed with Heparinized Hematocrit Tubes. Serum was separated by centrifugation and IL-17A expression in serum was measured by ELISA. PBMCs and spleen cells were analyzed by flow cytometry for IL-17A expression as described in *Flow Cytometry* below.

Experimental Autoimmune Encephalomyelitis (EAE) Model—Age matched 10–12-week-old *Rag1*$^{-/-}$ female mice were adoptively transferred with WT or *Rip2*−/− $CD4^+$ T cells ($2–3\times10^6$ cells) that were isolated from age matched female mice using a $CD4^+$ T cell Isolation kit (STEMCELL EasySep kit). The next day EAE was induced using $MOG_{35–55}$ and Complete Freund's Adjuvant (CFA) Emulsion Pertussis Toxin (PTX) kit (Hooke Laboratories) according to manufactures instructions. EAE clinical symptoms were blindly scored daily from day 7–26 after $MOG_{35–55}$ immunization according to EAE scoring guidelines (Hooke Laboratories).

$CD4^+$ T cell Differentiation and Treatment—Naïve $CD4^+$ T cells were isolated from the spleen of age and sex matched 6–10-week-old mice (STEMCELL EasySep kit). Cells were plated into plates coated with anti-CD3 and anti-CD28 in the presence of human rTGF-β (10 ng/ml) and mouse rIL-6 (20 ng/ml) for conventional Th17 cells or mouse rIL-1β (40 ng/ml), mouse rIL-6 (20 ng/ml) and mouse rIL-23 (50 ng/ml) for pathogenic Th17 cells in

the presence of anti-mouse IFN-y (10 μg/ml) and anti-mouse IL-4 (5 μg/ml). For iTreg cell differentiation, naïve $CD4^+$ T cells were cultured with plate-bound anti-CD3 and anti-CD28 antibodies and recombinant TGF-β (5 ng/ml). For experiments analyzing cytokine expression by ELISA, supernatant was collected on day 5. Cells were analyzed on day 3 for intracellular cytokine expression, RORα expression or FOXP3 expression as detailed in *Flow Cytometry* below. For experiments analyzing gene expression by qPCR, cells were harvested on day 3. For dNP2-FLAG and dNP2-CARD-FLAG peptide treatment of pTh17 cells, 15μM or indicated dose of peptide was added at day 0 and day 2 of differentiation. On day 3 cells were either harvested for RNA extraction and qPCR or analyzed by flow cytometry for IL-17A expression. For treatment of cells with RIP2 Kinase inhibitors, cells were stimulated with OD36 (200 nM) or GSK583 (20 nM) at day 0 and day 2 of differentiation and analyzed on day 3 by flow cytometry for IL-17A expression. All cell culture was performed at 37 °C in 5% CO_2.

Generation of Bone Marrow Dendritic Cells (BMDC)—Bone marrow cells were cultured in the presence of rGM-CSF (20 ng/ml) to differentiate to BMDC. Media and cytokines were replenished at day 3 and day 6. Cells were harvested at day 10 and further isolated using the $CD11c^+$ isolation kit (Miltenyi Biotec). Cell culture was performed at 37 ° C in 5% CO_2.

Co-culture of $CD4^+$ T cells with BMDC—$CD4^+$ T cells were isolated from the spleen with a mouse $CD4^+$ T cell isolation kit (Miltenyi Biotec). $CD4^+$ T cells were co-cultured with BMDC at a ratio of 10:1 under pTh17 cell differentiation conditions. Supernatants were collected on day 3 of culture and production of IFN-γ and IL-17A were measured by ELISA. Cell culture was performed at 37 ° C in 5% CO_2.

Treg cells suppression assay—Treg cells ($CD4^+CD25^+$) were isolated from spleen and lymph node of age matched male and female mice by cell sorting. $FOXP3^+$ percentages were confirmed by flow cytometry (>97%). Splenic T cells were labelled with CSFE and co-cultured with Treg cells in plates coated with anti-CD3 and anti-CD28 for 3 days. CSFE expression in $CD3^+CD4^+$ cells was analyzed by flow cytometry. Cell culture was performed at 37 ° C in 5% CO_2.

siRNA mediated gene silencing—Naïve $CD4^+$ T cells were plated onto anti-CD3 and anti-CD28 coated plates with 12.5 ng/ml mouse rIL-2, anti-IFN-y (10 μg/ml) and anti-IL-4 (5 μg/ml) for 16–18 hours (culture media: IMDM with 10% FBS). Media was then removed and replaced with Accell Delivery Medium (Dharmacon) containing 10% delipidated FBS and cells were differentiated under pathogenic Th17 cell conditions with the addition of 1.5 μM of Accell control siRNA or siRNA targeted to murine si*Rora* and/or si*Rip2* (Dharmacon). After 48 hours; culture media was replaced with fresh pTh17 cell condition media (IMDM containing 5% FBS). Next day, cells were harvested for qPCR or analyzed by flow cytometry for IL-17A expression.

Retrovirus production and T cell transduction—The sequence encoding human Rip2 from the pUNO1-hRIPK2 vector was cloned into pMIGR1(EGFP) to generate pMIGR1-hRip2. From this plasmid, the change-IT Mutagenesis kit was used to generate

pMIGR-hRip2ΔCARD (RIP2 CARD domain deletion (1–143)), pMIGR1-hRip2K47A (RIP2 K47A mutation) and pMIGR1-hRip2.CARD (RIP2 CARD domain only). *Rip2* shRNA (TRCN0000022485) was cloned into pMKO.1(-GFP) to generate pMKO.1-RIP2sh. Plasmids and pVSV-G were co-transfected into GP2–293 cells (Clonetech) with lipofectamine (Invitrogen). Retrovirus containing culture supernatant was collected at 48 hrs and 72 hrs post transfection. Naïve $CD4^+$ T cells were activated with anti-CD3 and anti-CD28 in the presence of 12.5 ng/ml mouse rIL-2, anti-IFN-y and anti-IL4 for 24 hours prior to retroviral infection. T cells were infected with retrovirus by centrifugation on RetroNectin (Takara) coated plates at varying multiplicities of infection (MOI). T cells were then cultured under pathogenic Th17 cell conditions. Retrovirus infected cells were sorted by GFP expression for qPCR analysis. Transduced T cells (GFP^+) were analyzed by flow cytometry for cytokine expression as detailed in *Flow Cytometry*.

Flow Cytometry Analysis—Flow cytometric analysis was performed on a LSR II (BD Biosciences) or a CyAn ADP Analyzer (Beckman Coulter, Inc.) and the data was analyzed by Summit (Dako, Carpentaria, CA, USA) or FlowJo (FlowJo, LLC, Ashland, OR). Flow sorting was performed on an Aria II or Aria III flow sorter (BD Biosciences). Anti-RORα was purchased from Abcam and conjugated with a FITC labeling kit (Thermo Fisher Scientific). All other antibodies were purchased from BioLegend, eBiosciences or TONBO as indicated in the Key Resource Table. For analysis of lung lymphocyte cytokine expression, cells were stimulated *ex vivo* with plate bound anti-CD3 and anti-CD28 for 24 hours in the presence of 3μg/ml Brefeldin A, then stained for surface antigens to detect $CD8^+$ T cells ($\beta TCR^+CD4^-CD8^+$), CD4+ T cells ($\beta TCR^+CD4^+CD8^-$), γδ T cells ($\gamma\delta TCR^+$) and NKT cells ($CD3^+NK1.1^+$). Following surface staining, cells were then fixed, permeabilized (BD) and stained for IL-17A and IFN-γ. For analysis of cytokine expression by ILC3's ($CD3^-Gr1^-CD4^-CD8^-B220^-\gamma\delta TCR^-NK1.1^-CD11c^-CD19^-FceRIa^-Thy1.1^+$), lung lymphocytes were stimulated with 50 ng/ml PMA and 1 μg/ml Ionomycin with 10 μg/ml Brefeldin A for 5–6 hours, stained for surface antigens then fixed, permeabilized (BD) and stained for IL-17A. For analysis of PBMC and spleen cell cytokine expression, cells were re-stimulated *ex vivo* with 50 ng/ml PMA and 1 μg/ml Ionomycin with 10 μg/ml Brefeldin A for 5–6 hours, stained for surface antigens to detect $CD8^+$ and $CD4^+$ T cells then fixed, permeabilized (BD) and stained for IL-17A. For analysis of lung neutrophil and T cell populations; cells were stained for surface antigens CD11b, Ly6G, CD3, CD4 and CD8. For assessment of cytokine production by *in vitro* derived Th17 cells, cells were stimulated with 50 ng/ml PMA and 1 μg/ml Ionomycin with 10 μg/ml Brefeldin A for 4 hours then stained for CD4 and a LIVE/DEAD fixable cell stain (Invitrogen). Cells were then fixed and permeabilized (BD) and stained for IL-17A. For assessment of FOXP3 expression or RORα and IL-17A expression, cells were fixed and permeabilized with FOXP3 staining kit (Thermo Fisher Scientific). For analysis of *Rip2* expression in lung $CD3^+CD4^+$ T cells, lung single cell suspensions harvested from CP infected *Ifng*$^{Thy1.1}$*Il17a*^{EGFP} reporter mice were treated with PMA (50 ng/ml) and Ionomycin (1 μg/ml) with 10 μg/ml Brefeldin A for 3 hours and stained with CD3, CD4 and Thy1.1 specific antibodies. For isolation of retrovirus infected cells for qPCR, cells were sorted based on GFP expression. For some experiments counting beads were added for calculation of cell numbers.

qPCR—qPCR was performed with SYBR green system (Bio-Rad) or the Power SYBR Green RNA-to-Ct 1 step kit (Thermo Fisher Scientific). qPCR was performed for *18S, Csf2, Hprt, Ifng, IL10, Il17a, Il1r1, Il23r, Rip2, Rora, Rorc* and *Tbx21* with primers listed in the Key Resource Table.

ChIP assay—ChIP assay was performed according to the manufacture's protocol of ChIP-IT High Sensitivity (Active Motif). Briefly, 7×10^6 *in vitro* differentiated pathogenic Th17 cells were cross-linked with 1% formaldehyde, then chromatin was sheared by sonication for 25 min (cycle of 30 sec on, 30 sec off). Chromatin was incubated with 4 μg of anti-RORα (ab60134, Abcam) or control rabbit IgG overnight at 4 °C and then incubated with pre-washed protein G agarose beads for 3 hrs. ChIP reactions were spun 1250 × g for 1 min, washed three times and immunoprecipitated DNA was purified. *Il17a* CNSs were analyzed by RT-PCR with SYBR green system (Bio-Rad) using primers for *Il17a* CNS1 and Il17a CNS2 listed in the Key Resource Table.

shRNA mediated silencing of RIP2 in Human $CD4^+$ T cells—Peripheral Blood Mononuclear Cells (PBMC) were isolated using Ficoll-Paque PLUS gradient (GE Healthcare). $CD4^+$ T cells were isolated using Dynal CD4 Positive Isolation Kit (Invitrogen). Purified cells were cultured in RPMI media containing 10% FBS and activated with anti-CD3 and anti-CD28 coated beads (Invitrogen) at a bead: cell ratio of 1:4 in media containing human rIL-2. VSV-G pseudotyped control or RIP2-shRNA (Sigma) containing viral particles were produced in HEK293T cells by calcium phosphate transfection according to the manufacturer's protocol (ProFection, Promega). Lentiviral supernatants were filtered, concentrated by centrifugation and filtered as previously described(Unutmaz et al., 1999). Cells were infected with lentiviral supernatants (at multiplicity of infection, MOI, of 5) at day 1 of activation. For intracellular cytokine staining, cells were activated with PMA (20 ng/ml for $CD4^+$ T cells and 40 ng/ml for PBMC) and Ionomycin (500 ng/ml) (Sigma Aldrich) in the presence of GolgiStop protein transport inhibitor (BD) for 4–6 hours. Cells were then stained for surface antigens CD3, CD4, CCR6 and CD45RO, then fixed and permeabilized (ebioscience) and stained for IL-17A. Immunoblot analysis was performed with anti-RIP2 (Abcam) and anti-RORα (Abcam) antibodies.

QUANTIFICATION AND STATISTICAL ANALYSIS

Statistical analyses of data are described in figure legends.

KEY RESOURCES TABLE

REAGENT or RESOURCE	SOURCE	IDENTIFIER
Antibodies		
Anti-human and mouse RIP2	Abcam	Cat # ab8428
Anti-human and mouse ROR alpha	Abcam	Cat # ab60134
Anti-human CCR6 – BV605 (clone G034E3)	BioLegend	Cat # 353420
Anti-human CD4 – FITC (clone A161A1)	BioLegend	Cat # 357406
Anti-human CD45RO- APC-Cy7 (clone UCHL1)	BioLegend	Cat # 304227

REAGENT or RESOURCE	SOURCE	IDENTIFIER
Anti-human IL-17A- BV421 (clone BL168)	BioLegend	Cat # 512322
Anti-mouse B220 – APC (clone RA3–6B2)	Tonbo Biosciences	Cat # 20-0452-U100
Anti-mouse C28 (clone 37.51)	BioXcell	Cat # BE001-1
Anti-mouse CD11b – PerCP/Cy5.5 (clone M1/70)	BioLegend	Cat # 101227
Anti-mouse CD11c – PerCP Cy5.5 (clone N418)	eBioscience	Cat # 45-0114-80
Anti-mouse CD19 – PerCp Cy5.5 (eBio1D3)	eBioscience	Cat # 45-0193-82
Anti-mouse CD25 – biotin (clone PC61.5)	Tonbo Biosciences	Cat # 30-0251-U500
Anti-mouse CD25 – PE (clone PC61.5)	eBioscience	Cat # 12-0251-82
Anti-mouse CD25 – PerCP/Cy5.5 (clone PC61.5)	Tonbo Biosciences	Cat # 65-0251-U100
Anti-mouse CD3ε – PerCP Cy5.5 (30-F11)	Tonbo Biosciences	Cat # 65-0031-U100
Anti-mouse CD3ε (clone 145–2C11)	BioXcell	Cat # BE015-1
Anti-mouse CD4 – APC (clone RM4–5)	eBioscience	Cat # 17-0042-82
Anti-mouse CD4 – APC/Cy7 (clone GK1.5)	Tonbo Biosciences	Cat # 25-0041-U100
Anti-mouse CD4 – PerCP Cy5.5 (RM4–5)	eBioscience	Cat # 65-0042-U025
Anti-mouse CD44 – biotin (clone IM7)	BioLegend	Cat # 103004
Anti-mouse CD44 – FITC (clone IM7)	eBioscience	Cat # 11-0441-85
Anti-mouse CD62L – APC (clone MEL-14)	eBioscience	Cat # 17-0621-81
Anti-mouse CD8a – APC (clone 53–6.7)	Tonbo Biosciences	Cat # 20-0081-U100
Anti-mouse FcRla – APC (clone N28.1)	eBioscience	Cat # 14-5847-82
Anti-mouse FOXP3 – PE (clone FJK-16s)	eBioscience	Cat # 12-5773-82
Anti-mouse GR1 – FITC (RB6–8C5)	eBioscience	Cat # 11-5931-82
Anti-mouse IFNg – FITC (clone XMG1.2)	BioLegend	Cat # 505806
Anti-mouse IFNg – PB (clone XMG1.2)	Tonbo Biosciences	Cat # 75-7311-U100
Anti-mouse IFNg (clone XMG1.2)	BioLegend	Cat # 505827
Anti-mouse IL-4 (clone 11B11)	BioLegend	Cat # 504122
Anti-mouse IL17A – APC (clone TC11–18H10.1)	BioLegend	Cat # 506916
Anti-mouse IL17A – PE (clone TC11–18H10.1)	BioLegend	Cat # 506903
Anti-mouse Ly6G – PE (clone 1A8)	BioLegend	Cat # 127607
Anti-mouse NK1.1 – APC (clone PK136)	eBioscience	Cat # 17-5941-82
Anti-mouse TCRβ – FITC (clone H57–597)	eBioscience	Cat # 11-5961-85
Anti-mouse TCRγ/δ – FITC (clone eBioGL3)	eBioscience	Cat # 11-5711-81
Anti-mouse Thy1.1 – APC (clone HiS51)	eBioscience	Cat # 47-0902-82
Anti-mouse Thy1.1 – eFlour450 (clone HiS51)	eBioscience	Cat # 48-0900-82
Rabbit IgG, polyclonal	Abcam	Cat # ab171870
Bacterial and Virus Strains		
Chlamydia pneumoniae CM-1	ATCC	VR-1360
AAV-PCSK9	University of Kentucky, Lexington, KY	Dr. Alan Daugherty
Biological Samples		
Healthy Adult Peripheral Blood		

REAGENT or RESOURCE	SOURCE	IDENTIFIER
Murine Aorta		
Murine BALF		
Murine Blood		
Murine Heart		
Murine Lung		
Murine Spleen		
Chemicals, Peptides, and Recombinant Proteins		
Recombinant mouse IL-1β	BioLegend	Cat # 575104
Recombinant mouse IL-23	BioLegend	Cat # 589004
Recombinant mouse IL-6	BioLegend	Cat # 575704
Recombinant mouse TGF-β1	BioLegend	Cat # 580704
Recombinant mouse TGF-β1	R&D Systems	Cat # 672808
Recombinant mouse IL-2	R&D Systems	Cat# 402-ML
Recombinant human IL-2	R&D Systems	Cat # 202-IL-010
Recombinant mouse GM-CSF	R&D Systems	Cat# 415-ML
dNP2-FLAG peptide	Life Tein	This Study
dNP2-CARD-FLAG	Life Tein	This Study
OD36	Millipore Sigma	Cat # 532757
GSK583	Cayman Chemical	Cat # 1346547-00-9
Anakinra (Kineret)	Sobi	N/A
LPS	Invivogen	Cat # Tlrl-3pelps
ChIP-IT High Sensitivity Kit	Active Motif	Cat # 35040
SMARTpool: Accell Rora siRNA	Dharmacon Inc.	Cat # E-040430-00-0020
SMARTpool: Accell Ripk2 siRNA	Dharmacon Inc.	Cat # E-052248-00-0010
Accell Non-targeting siRNA #1	Dharmacon Inc.	Cat # D-001910-01-20
Accell siRNA Delivery Media	Dharmacon Inc.	Cat # B-005000-500
delipidated FBS	Gemini	Cat # 900-123
RetroNectin	Clontech	Cat # T100B
Lipofectamine	Invitrogen	Cat # 11668019
Brefeldin A	Sigma Aldrich	Cat # B6542
PMA	Sigma Aldrich	Cat # P1585
Ionomycin	Cayan Chemical Company	Cat # 10004974
Fixable Viability Dye eFluor 506	eBioscience	Cat # 65-0866-14
Liberase	Sigma Aldrich	Cat # 540112001
DNase1	Sigma Aldrich	Cat # 10104159001
RBC Lysis Buffer	eBioscience	Cat # 652876
GolgiStop	BD	Cat # 554724
Human T-activator CD3CD28 Dynabeads	Thermo Fisher	Cat # 111.61D
Critical Commercial Assays		

REAGENT or RESOURCE	SOURCE	IDENTIFIER
$CD11c^+$ Isolation kit	Miltenyi Biotec	Cat # 130-108-338
$CD4^+$ T-cell Isolation Kit	Miltenyi Biotec	Cat # 130-104-454
CellTrace CFSE Cell Proliferation Kit	Invitrogen	Cat # C34554
CellTrace Violet Cell Proliferation Kit	Invitrogen	Cat # C34557
Change-IT Mutagenesis kit	Affymetrix USB	Cat # 784801 KT
Dynal $CD4^+$ Isolation kit	Thermo Fisher	Cat # 111331D
EasySep Mouse $CD4^+$ T cell Isolation Kit	STEMCELL Technologies	Cat # 19852
EasySep Mouse naïve $CD4^+$ T cell Isolation Kit	STEMCELL Technologies	Cat # 19765
Fixation/Permeabilization Solution Kit	BD Biosciences	Cat # 554714
Mouse IFN gamma ELISA	eBioscience	Cat # 88-7314-88
Mouse IL-17A ELISA	eBioscience	Cat # 88-7371-88
Mouse IL-17A and F heterodimer ELISA	eBioscience	Cat # 88-8711-88
Mouse IL17-F ELISA	eBioscience	Cat # 88-7472-88
Pathfinder Chlamydia Culture Confirmation System	Bio-Rad	Cat # 30701
Power SYBR Green RNA-to-CT 1-Step Kit	Thermo Fisher	Cat # 4389986
ProFection Kit	Promega	Cat # E1200
Retro-X Universal Packaging System	Clontech	Cat # 631530
Rneasy Plus Mini Kit	Qiagen	Cat # 74136
Deposited Data		
N/A		
Experimental Models: Cell Lines		
HEp-2	ATCC	CCL-23
GP2–293	Clontech	Cat # 631530
Experimental Models: Organisms/Strains		
C57BL/6J	The Jackson Laboratory	Stock 000664
Rip2$^{-/-}$	University of California, Los Angeles, CA	Dr. Genhong Cheng
Il17$^{-/-}$	University of Tokyo, Tokyo.	Dr. Yoichiro Iwakura
Rip2$^{-/-}$*Il17*$^{-/-}$	Cedars Sinai Medical Center, Los Angeles, CA	This paper
Rag1$^{-/-}$	The Jackson Laboratory	Stock 002216
Nod2$^{-/-}$	The Jackson Laboratory	Stock 005763
Nod1$^{-/-}$*Nod2*$^{-/-}$	University of California Davis, Davis, CA	Dr. Andreas J. Baulmer
Ldlr$^{-/-}$	The Jackson Laboratory	Stock 002207
Ifng$^{Thy1.1}$*Il17a*^{EGFP}	Cedars Sinai Medical Center, Los Angeles, CA	Dr. Masayuki Fukata
Oligonucleotides		
18S fwd: TCAAGAACGAAAGTCGGAGG		
18S rev: GGACATCTAAGGGCATCACA		
Csf2 fwd: TCGTCTCTAACGAGTTCTCCTT		

REAGENT or RESOURCE	SOURCE	IDENTIFIER
Csf2 rev: CGTAGACCCTGCTCGAATATCT		
Hprt fwd: CTCATGGACTGATTATGGACAGGAC		
Hprt rev: GCAGGTCAGCAAAGAACTTATAGCC		
Ifng fwd: GCCACGGCACAGTCATTGA		
Ifng rev: TGCTGATGGCCTGATTGTCTT		
Il10 fwd: GCTGGACAACATACTGCTAACC		
Il10 rev: ATTTCCGATAAGGCTTGGCAA		
Il17a CNS1 fwd: TCTTCAAGGCCCCAAACTAGG		
Il17a CNS1 rev: TGCCCCCATTGAGGAGCATA		
Il17a CNS2 fwd: AGATAACCCAACCACAGCGT		
Il17a CNS2 rev: GGAGGCGCATGCAAATTCTT		
Il17a fwd: CTCCAGAAGGCCCTCAGACTA		
Il17a rev: AGCTTTCCCTCCGCATTGACA		
Il1r1 fwd: GTGCTACTGGGGCTCATTTGT		
Il1r1 rev: GGAGTAAGAGGACACTTGCGAAT		
Il23r fwd: AAGGCTTTTCGGAACCTCAT		
Il23r rev: TTCCAGGTGCATGTCATGTT		
Rip2 fwd: CGTGTGGATCCTCTCTGCTC		
Rip2 rev: AGTGGTGTGCCTTCAACGAA		
Rora fwd: TCTCCCTGCGCTCTCCGCAC		
Rora rev: TCCACAGATCTTGCATGGA		
Rorc fwd: TGCAGGAGTAGGCCACATTAC		
Rorc rev: CCGCTGAGAGGGCTTCAC		
Tbx21 fwd: CAACAACCCCTTTGCCAAAG		
Tbx21 rev: TCCCCCAAGCAGTTGACAGT		
Recombinant DNA		
pMIGR	Addgene	Plasmid # 27490
pMIGR-RIP2	This paper	N/A
pMIGR-RIP2ΔCARD	This paper	N/A
pMIGR-RIP2K47A	This paper	N/A
pMIGR-RIP2.CARD	This paper	N/A
pMKO.1	Addgene	Plasmid # 10676
pMKO.1-RIP2sh	This paper	N/A
pVSVG	Clontech	Cat # 631530
pUNO1-hRIPK2	Invivogen	Cat # puno1-hrick
Software and Algorithms		
FlowJo Software	FlowJo LLC	
GraphPad Prism	GraphPad Software, Inc.	
Summitt Software System	Cytomation	

REAGENT or RESOURCE	SOURCE	IDENTIFIER
Other		
High fat diet	Harlan Teklad	Cat # TD88137
75 mm Hematocrit Tubes	Fisher Scientific	Cat # 21-176-6

Supplementary Material

Refer to Web version on PubMed Central for supplementary material.

ACKNOWLEDGEMENTS

We thank Wenxuan Zhang, Ganghua Huang, Malcolm Lane for their excellent technical assistance. We thank Dr. Masayuki Fukata at Cedars-Sinai Medical Center for *Ifng*$^{Thy1.1}$ *Il17a*^{EGFP} mice. We thank Dr. Jay K. Kolls (Univ. of Pittsburgh) and Dr. Yoichiro Iwakura (Tokyo Univ. of Science) for kindly providing *Il17a*$^{-/-}$ mice. We thank Dr. Andreas J. Baumler (Univ. California Davis, Davis, CA) for kindly providing *Nod1*$^{-/-}$ *Nod2*$^{-/-}$ mice. We also thank Polly Sun for technical assistance. We thank Dr. Alan Daugherty (Univ. Kentucky) for kindly providing AAV-PCSK9. This work was supported by National Institutes of Health (NIH) grants AI067995, 2R56AI067995–06, and AI117968 to M.A, HL111483–01 to S.C, AI112826 to T.R.C and American Heart Association 09BGIA2060145 to S.C.

References

Aujla SJ, Chan YR, Zheng M, Fei M, Askew DJ, Pociask DA, Reinhart TA, McAllister F, Edeal J, Gaus K, et al. (2008). IL-22 mediates mucosal host defense against Gram-negative bacterial pneumonia. Nat Med 14, 275–281. [PubMed: 18264110]

Balamayooran T, Batra S, Balamayooran G, Cai S, Kobayashi KS, Flavell RA, and Jeyaseelan S (2011). Receptor-interacting protein 2 controls pulmonary host defense to Escherichia coli infection via the regulation of interleukin-17A. Infect Immun 79, 4588–4599. [PubMed: 21844230]

Barros-Martins J, Schmolka N, Fontinha D, Pires de Miranda M, Simas JP, Brok I, Ferreira C, Veldhoen M, Silva-Santos B, and Serre K (2016). Effector gammadelta T Cell Differentiation Relies on Master but Not Auxiliary Th Cell Transcription Factors. J Immunol 196, 3642–3652. [PubMed: 26994218]

Butcher MJ, Gjurich BN, Phillips T, and Galkina EV (2012). The IL-17A/IL-17RA Axis Plays a Proatherogenic Role via the Regulation of Aortic Myeloid Cell Recruitment. Circulation Research.

Chen S, Shimada K, Zhang W, Huang G, Crother TR, and Arditi M (2010a). IL-17A is proatherogenic in high-fat diet-induced and Chlamydia pneumoniae infection-accelerated atherosclerosis in mice. J Immunol 185, 5619–5627. [PubMed: 20935201]

Chen SA, Shimada K, Zhang W, Huang GH, Crother TR, and Arditi M (2010b). IL-17A Is Proatherogenic in High-Fat Diet-Induced and Chlamydia pneumoniae Infection-Accelerated Atherosclerosis in Mice. Journal of Immunology 185, 5619–5627.

Chin AI, Dempsey PW, Bruhn K, Miller JF, Xu Y, and Cheng G (2002). Involvement of receptor-interacting protein 2 in innate and adaptive immune responses. Nature 416, 190–194. [PubMed: 11894097]

Chung Y, Chang SH, Martinez GJ, Yang XO, Nurieva R, Kang HS, Ma L, Watowich SS, Jetten AM, Tian Q, and Dong C (2009). Critical regulation of early Th17 cell differentiation by interleukin-1 signaling. Immunity 30, 576–587. [PubMed: 19362022]

Duewell P, Kono H, Rayner KJ, Sirois CM, Vladimer G, Bauernfeind FG, Abela GS, Franchi L, Nuñez G, Schnurr M, et al. (2010). NLRP3 inflammasomes are required for atherogenesis and activated by cholesterol crystals. Nature 464, 1357–1361. [PubMed: 20428172]

Fairhead T, Lian D, McCully ML, Garcia B, Zhong R, and Madrenas J (2008). RIP2 is required for NOD signaling but not for Th1 cell differentiation and cellular allograft rejection. Am J Transplant 8, 1143–1150. [PubMed: 18522545]

Gao Q, Jiang Y, Dai S, Wang B, Gao F, Guo C, Zhu F, Wang Q, Wang X, Wang J, et al. (2012). Interleukin 17A Exacerbates Atherosclerosis by Promoting Fatty Acid-Binding Protein 4-Mediated ER Stress in Macrophages. Circulation Research.

Ghoreschi K, Laurence A, Yang XP, Tato CM, McGeachy MJ, Konkel JE, Ramos HL, Wei L, Davidson TS, Bouladoux N, et al. (2010). Generation of pathogenic T(H)17 cells in the absence of TGF-β signalling. Nature 467, 967–971. [PubMed: 20962846]

Girardin SE, Travassos LH, Hervé M, Blanot D, Boneca IG, Philpott DJ, Sansonetti PJ, and Mengin-Lecreulx D (2003). Peptidoglycan molecular requirements allowing detection by Nod1 and Nod2. J Biol Chem 278, 41702–41708. [PubMed: 12871942]

Hall HT, Wilhelm MT, Saibil SD, Mak TW, Flavell RA, and Ohashi PS (2008). RIP2 contributes to Nod signaling but is not essential for T cell proliferation, T helper differentiation or TLR responses. Eur J Immunol 38, 64–72. [PubMed: 18085666]

Huang W, Na L, Fidel PL, and Schwarzenberger P (2004). Requirement of interleukin-17A for systemic anti-Candida albicans host defense in mice. J Infect Dis 190, 624–631. [PubMed: 15243941]

Ishigame H, Kakuta S, Nagai T, Kadoki M, Nambu A, Komiyama Y, Fujikado N, Tanahashi Y, Akitsu A, Kotaki H, et al. (2009). Differential roles of interleukin-17A and −17F in host defense against mucoepithelial bacterial infection and allergic responses. Immunity 30, 108–119. [PubMed: 19144317]

Ivanov II, Frutos R.e.L., Manel N, Yoshinaga K, Rifkin DB, Sartor RB, Finlay BB, and Littman DR. (2008). Specific microbiota direct the differentiation of IL-17-producing T-helper cells in the mucosa of the small intestine. Cell Host Microbe 4, 337–349. [PubMed: 18854238]

Jäger A, Dardalhon V, Sobel RA, Bettelli E, and Kuchroo VK (2009). Th1, Th17, and Th9 effector cells induce experimental autoimmune encephalomyelitis with different pathological phenotypes. The Journal of Immunology 183, 7169–7177. [PubMed: 19890056]

Keestra-Gounder AM, Byndloss MX, Seyffert N, Young BM, Chávez-Arroyo A, Tsai AY, Cevallos SA, Winter MG, Pham OH, Tiffany CR, et al. (2016). NOD1 and NOD2 signalling links ER stress with inflammation. Nature 532, 394–397. [PubMed: 27007849]

Kelly MN, Kolls JK, Happel K, Schwartzman JD, Schwarzenberger P, Combe C, Moretto M, and Khan IA (2005). Interleukin-17/interleukin-17 receptor-mediated signaling is important for generation of an optimal polymorphonuclear response against Toxoplasma gondii infection. Infect Immun 73, 617–621. [PubMed: 15618203]

Kobayashi K, Inohara N, Hernandez LD, Galán JE, Núñez G, Janeway CA, Medzhitov R, and Flavell RA (2002). RICK/Rip2/CARDIAK mediates signalling for receptors of the innate and adaptive immune systems. Nature 416, 194–199. [PubMed: 11894098]

Komiyama Y, Nakae S, Matsuki T, Nambu A, Ishigame H, Kakuta S, Sudo K, and Iwakura Y (2006). IL-17 plays an important role in the development of experimental autoimmune encephalomyelitis. J Immunol 177, 566–573. [PubMed: 16785554]

Legrand-Poels S, Kustermans G, Bex F, Kremmer E, Kufer TA, and Piette J (2007). Modulation of Nod2-dependent NF-kappaB signaling by the actin cytoskeleton. J Cell Sci 120, 1299–1310. [PubMed: 17356065]

Levin MC, Jirholt P, Wramstedt A, Johansson ME, Lundberg AM, Trajkovska MG, Ståhlman M, Fogelstrand P, Brisslert M, Fogelstrand L, et al. (2011). Rip2 deficiency leads to increased atherosclerosis despite decreased inflammation. Circ Res 109, 1210–1218. [PubMed: 21959219]

Li L, Wang X, Chen W, Qi H, Jiang DS, Huang L, Huang F, Wang L, Li H, and Chen X (2015). Regulatory role of CARD3 in left ventricular remodelling and dysfunction after myocardial infarction. Basic Res Cardiol 110, 56. [PubMed: 26463597]

Lim S, Kim WJ, Kim YH, Lee S, Koo JH, Lee JA, Yoon H, Kim DH, Park HJ, Kim HM, et al. (2015). dNP2 is a blood-brain barrier-permeable peptide enabling ctCTLA-4 protein delivery to ameliorate experimental autoimmune encephalomyelitis. Nature communications 6, 8244.

Lupfer C, Thomas PG, Anand PK, Vogel P, Milasta S, Martinez J, Huang G, Green M, Kundu M, Chi H, et al. (2013). Receptor interacting protein kinase 2-mediated mitophagy regulates inflammasome activation during virus infection. Nat Immunol 14, 480–488. [PubMed: 23525089]

Miossec P, and Kolls JK (2012). Targeting IL-17 and T(H)17 cells in chronic inflammation. Nat Rev Drug Discov 11, 763–776. [PubMed: 23023676]

Mosolygó T, Korcsik J, Balogh EP, Faludi I, Virók DP, Endrész V, and Burián K (2013). Chlamydophila pneumoniae re-infection triggers the production of IL-17A and IL-17E, important regulators of airway inflammation. Inflamm Res 62, 451–460. [PubMed: 23385305]

Nembrini C, Reissmann R, Kopf M, and Marsland BJ (2008). Effective T-cell immune responses in the absence of the serine/threonine kinase RIP2. Microbes Infect 10, 522–530. [PubMed: 18403232]

Ogura Y, Inohara N, Benito A, Chen FF, Yamaoka S, and Nunez G (2001). Nod2, a Nod1/Apaf-1 family member that is restricted to monocytes and activates NF-kappaB. J Biol Chem 276, 4812–4818. [PubMed: 11087742]

Park JH, Kim YG, McDonald C, Kanneganti TD, Hasegawa M, Body-Malapel M, Inohara N, and Núñez G (2007). RICK/RIP2 mediates innate immune responses induced through Nod1 and Nod2 but not TLRs. J Immunol 178, 2380–2386. [PubMed: 17277144]

Patel DD, and Kuchroo VK (2015). Th17 Cell Pathway in Human Immunity: Lessons from Genetics and Therapeutic Interventions. Immunity 43, 1040–1051. [PubMed: 26682981]

Roche-Molina M, Sanz-Rosa D, Cruz FM, García-Prieto J, López S, Abia R, Muriana FJG, Fuster V, Ibáñez B, and Bernal JA (2015). Induction of sustained hypercholesterolemia by single adeno-associated virus-mediated gene transfer of mutant hPCSK9. Arteriosclerosis, Thrombosis, and Vascular Biology 35, 50–59.

Ruefli-Brasse AA, Lee WP, Hurst S, and Dixit VM (2004). Rip2 participates in Bcl10 signaling and T-cell receptor-mediated NF-kappaB activation. J Biol Chem 279, 1570–1574. [PubMed: 14638696]

Shaw PJ, Barr MJ, Lukens JR, McGargill MA, Chi H, Mak TW, and Kanneganti TD (2011). Signaling via the RIP2 adaptor protein in central nervous system-infiltrating dendritic cells promotes inflammation and autoimmunity. Immunity 34, 75–84. [PubMed: 21236705]

Shimada K, Chen S, Dempsey PW, Sorrentino R, Alsabeh R, Slepenkin AV, Peterson E, Doherty TM, Underhill D, Crother TR, and Arditi M (2009). The NOD/RIP2 pathway is essential for host defenses against Chlamydophila pneumoniae lung infection. PLoS Pathog 5, e1000379. [PubMed: 19360122]

Shimada K, Crother TR, and Arditi M (2012). Innate immune responses to Chlamydia pneumoniae infection: role of TLRs, NLRs, and the inflammasome. Microbes Infect 14, 1301–1307. [PubMed: 22985781]

Shimada K, Crother TR, Karlin J, Chen S, Chiba N, Ramanujan VK, Vergnes L, Ojcius DM, and Arditi M (2011). Caspase-1 dependent IL-1β secretion is critical for host defense in a mouse model of Chlamydia pneumoniae lung infection. PLoS One 6, e21477. [PubMed: 21731762]

Stockinger B, and Omenetti S (2017). The dichotomous nature of T helper 17 cells. Nat. Rev. Immunol 17, 535–544. [PubMed: 28555673]

Tumurkhuu G, Shimada K, Dagvadorj J, Crother TR, Zhang W, Luthringer D, Gottlieb RA, Chen S, and Arditi M (2016). Ogg1-Dependent DNA Repair Regulates NLRP3 Inflammasome and Prevents Atherosclerosis. Circ Res 119, e76–90. [PubMed: 27384322]

Unutmaz D, KewalRamani VN, Marmon S, and Littman DR (1999). Cytokine signals are sufficient for HIV-1 infection of resting human T lymphocytes. J Exp Med 189, 1735–1746. [PubMed: 10359577]

Veldhoen M, Hocking RJ, Atkins CJ, Locksley RM, and Stockinger B (2006). TGFbeta in the context of an inflammatory cytokine milieu supports de novo differentiation of IL-17-producing T cells. Immunity 24, 179–189. [PubMed: 16473830]

Wright JF, Guo Y, Quazi A, Luxenberg DP, Bennett F, Ross JF, Qiu Y, Whitters MJ, Tomkinson KN, Dunussi-Joannopoulos K, et al. (2007). Identification of an interleukin 17F/17A heterodimer in activated human CD4+ T cells. J Biol Chem 282, 13447–13455. [PubMed: 17355969]

Yang XO, Pappu BP, Nurieva R, Akimzhanov A, Kang HS, Chung Y, Ma L, Shah B, Panopoulos AD, Schluns KS, et al. (2008). T helper 17 lineage differentiation is programmed by orphan nuclear receptors ROR alpha and ROR gamma. Immunity 28, 29–39. [PubMed: 18164222]

Ye P, Rodriguez FH, Kanaly S, Stocking KL, Schurr J, Schwarzenberger P, Oliver P, Huang W, Zhang P, Zhang J, et al. (2001). Requirement of interleukin 17 receptor signaling for lung CXC

chemokine and granulocyte colony-stimulating factor expression, neutrophil recruitment, and host defense. J Exp Med 194, 519–527. [PubMed: 11514607]

Yosef N, Shalek AK, Gaublomme JT, Jin H, Lee Y, Awasthi A, Wu C, Karwacz K, Xiao S, Jorgolli M, et al. (2013). Dynamic regulatory network controlling TH17 cell differentiation. Nature 496, 461–468. [PubMed: 23467089]

HIGHLIGHTS

- RIP2 deficiency in $CD4^+$ T cells leads to severe IL-17A mediated diseases
- RIP2 suppresses pathogenic Th17 cell and supports conventional Th17 cell polarization
- RIP2 suppression of pathogenic Th17 cell differentiation is RORα and IL-1 dependent
- RIP2 CARD domain regulates pathogenic Th17 cell differentiation in $CD4^+$ T cells

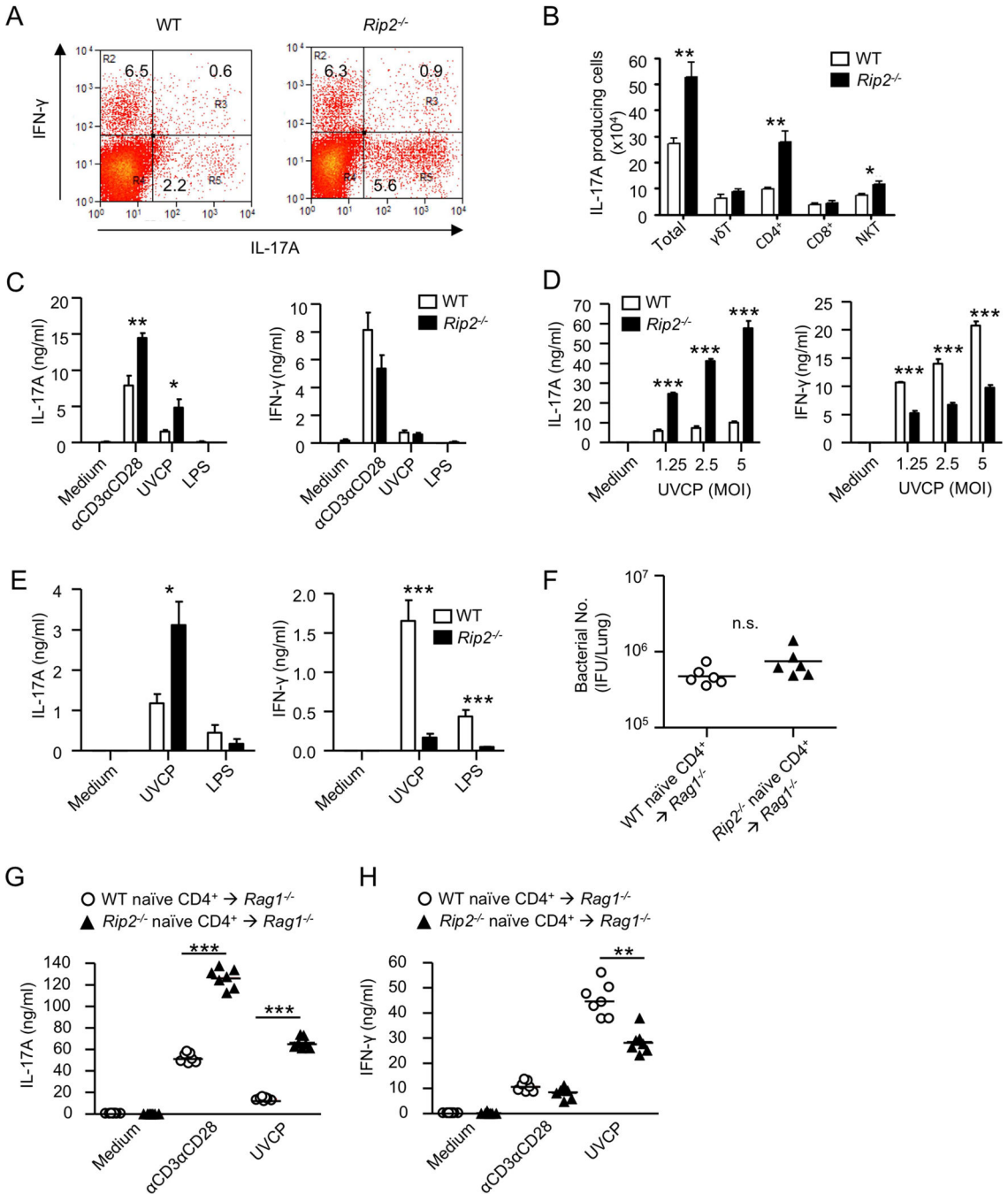

Figure 1. RIP2 deficiency enhances IL-17A production in CD4$^+$ T cells.

WT and *Rip2*$^{-/-}$ mice were intratracheally infected with *C. pneumoniae* (1×10^6 IFU). (A) Flow cytometry plots of IL-17A and IFN-γ producing lung CD4$^+$ T cells harvested 21 days p.i.. (B) The number of lung IL-17A producing cells harvested 21 days p.i.. (C and D) IL-17A and IFN-γ production in culture supernatant of MLN harvested 21 days p.i. and stimulated *ex vivo* with anti-CD3 and anti-CD28 Ab, UVCP (MOI 5, or as indicated) or LPS (100 ng/ml). (E) IL-17A and IFN-γ production in culture supernatant of splenocytes harvested 5 days p.i. and co-cultured with UVCP (MOI 5) pre-loaded or LPS (100 ng/ml)

pre-stimulated WT BMDC. (F) Bacterial load in lungs of *C. pneumoniae* infected *Rag1*$^{-/-}$ mice adoptively transferred with WT or *Rip2*$^{-/-}$ naïve CD4^{+} T cells. (G and H) IL-17A and IFN-γ production in culture supernatant of MLN, harvested 5 days p.i. from *Rag1*$^{-/-}$ mice adoptively transferred with WT or *Rip2*$^{-/-}$ naïve CD4^{+} T cells and stimulated *ex vivo* with anti-CD3 and anti-CD28 Ab or UVCP. Data are representative of three independent experiments (n=5–7 mice/group). Statistical analyses: Student's *t*-test. $*$ $p < 0.05$, $**$ $p < 0.01$, $***$ $p < 0.001$. Results are represented as mean ± SEM. See also Figure S1.

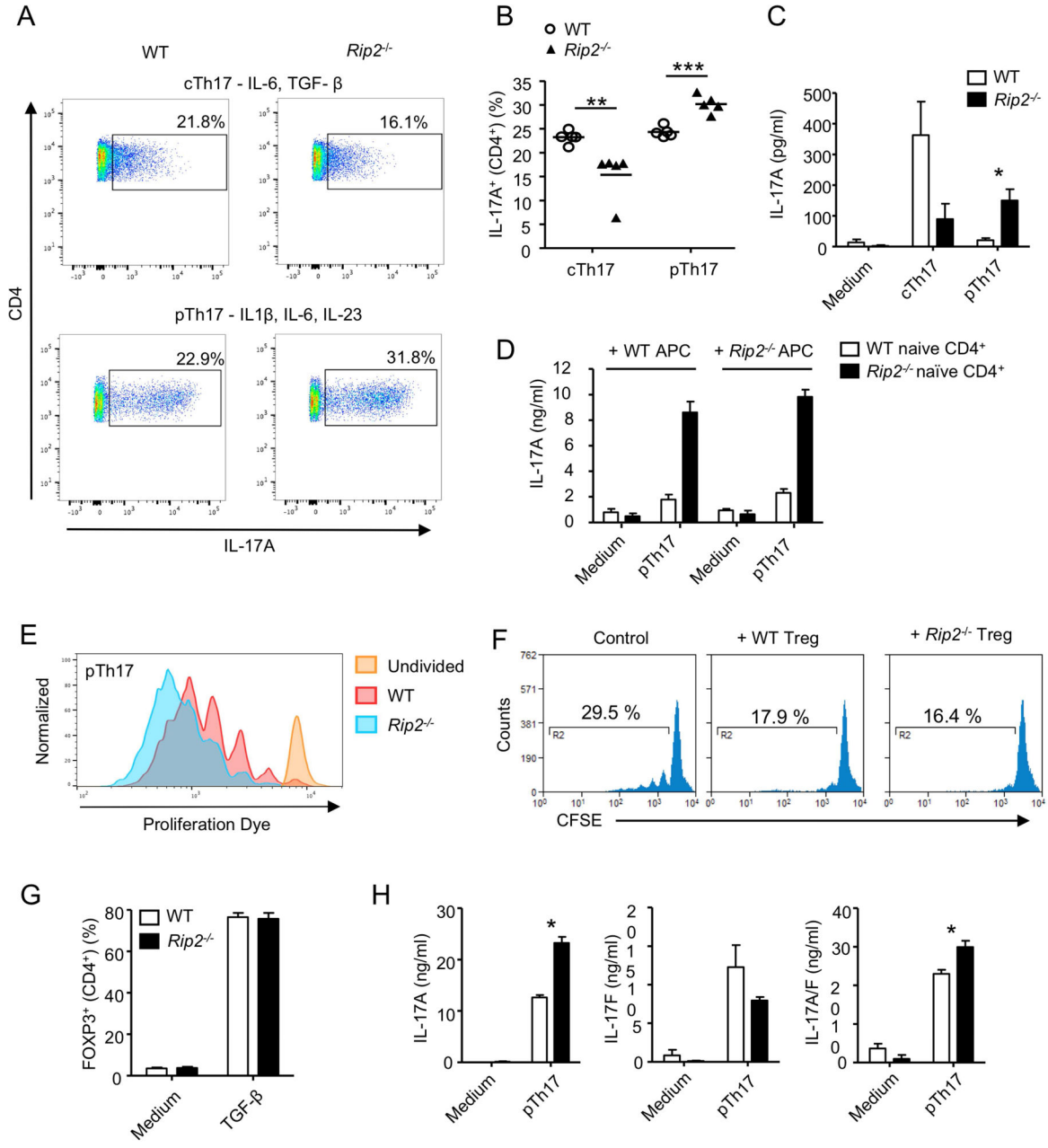

Figure 2. RIP2 deficient naïve CD4$^+$ T cells skew towards pathogenic Th17 cells.

Splenic naïve CD4$^+$ T cells from WT and *Rip2*$^{-/-}$ mice were differentiated *in vitro* into cTh17 cells, pTh17 cells, or Treg cells unless otherwise specified. (A) Flow cytometry plots of the percent of IL-17A expressing CD4$^+$ T cells differentiated under cTh17 cell or pTh17 cell conditions. (B) Percent of IL-17A expression in CD4$^+$ T cells differentiated under cTh17 cell or pTh17 cell conditions. Data are representative of four independent experiments (n=5–6). (C) IL-17A concentration in the culture supernatant of CD4$^+$ T cells differentiated under cTh17 cell or pTh17 cell conditions. (D) IL-17A concentration in the culture supernatant when CD4$^+$ T cells are co-cultured with WT or *Rip2*$^{-/-}$ BMDC under pTh17 cell conditions. (E) Flow cytometry plots of CellTrace-labeled cells differentiated *in*

vitro under pTh17 cell conditions. (F) Flow cytometry plots of CFSE-labeled T cell enriched splenocytes co-cultured with WT or *Rip2*$^{-/-}$ regulatory T cells in the presence of anti-CD3 and anti-CD28 Ab. (G) Percent of FOXP3 expressing CD4^{+} T cells differentiated under Treg cell conditions. (H) IL-17A, IL-17F and IL-17A and F heterodimer concentrations in the culture supernatant of cells differentiated under pTh17 cell conditions. Data are representative of two to three independent experiments (n=3–6 mice/group). Statistical analyses: Student's *t*-test. $*$ $p < 0.05$, $**$ $p < 0.01$, $***$ $p < 0.001$. Results are represented as mean ± SEM. See also Figure S2.

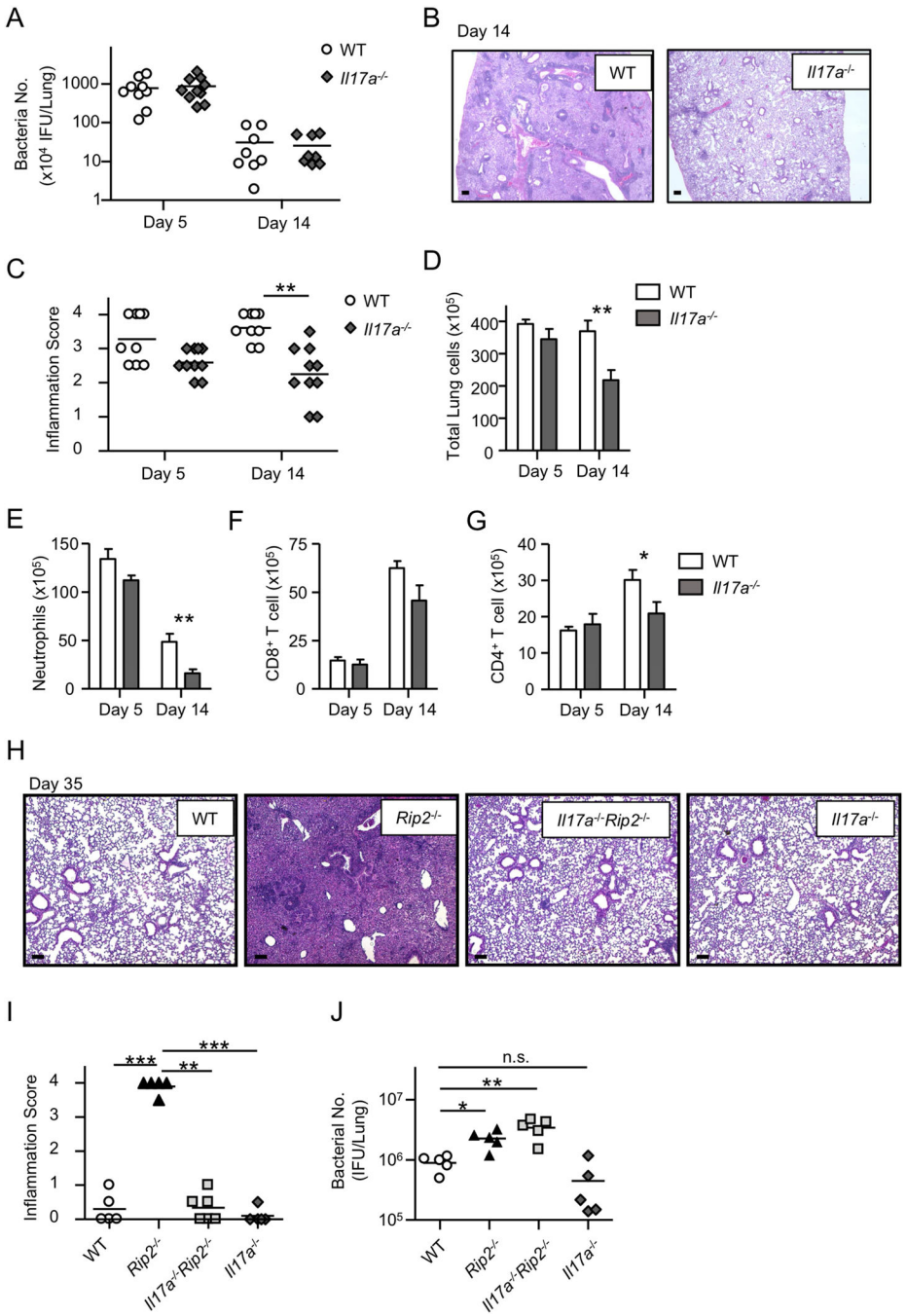

Figure 3: IL-17A is required for pathogenesis of *C. pneumoniae* induced lung inflammation in RIP2 deficient mice, but not bacterial clearance.

WT, *Rip2*$^{-/-}$, *Il17a*$^{-/-}$ *and Il17a*$^{-/-}$*Rip2*$^{-/-}$ mice were infected intratracheally with *C. pneumoniae* (1×10^6 IFU). (A) Bacterial load in lungs at day 5 and 14 p.i.. (B) H&E stained lung pathologies at day 14 p.i.. Scale bars represent 200 μm. (C) Lung inflammation score at days 5 and 14 p.i.. (D-G) The numbers of total lung cells, neutrophils ($Cd11b^+Ly6G^+$), $CD4^+$ and $CD8^+$ T cells in the lungs at day 5 and 14 p.i.. Data are representative of two independent experiments combined (n=9–10 mice/group). (H) H&E stained lung pathologies at day 35 p.i.. Scale bars represent 200 μm. (I) Lung inflammation scores at day

35 p.i.. (J) Bacterial load in lungs at day 5 p.i.. Data are representative of two independent experiments (n=5 mice/group). Statistical analyses: Student's *t*-test (A, C-G), one-way ANOVA followed by Tukey's post-hoc test (I) or one-way ANOVA followed by Dunett's post-hoc test (J). * $p < 0.05$, ** $p < 0.01$, *** $p < 0.001$. Results are represented as mean ± SEM. See also Figure S3.

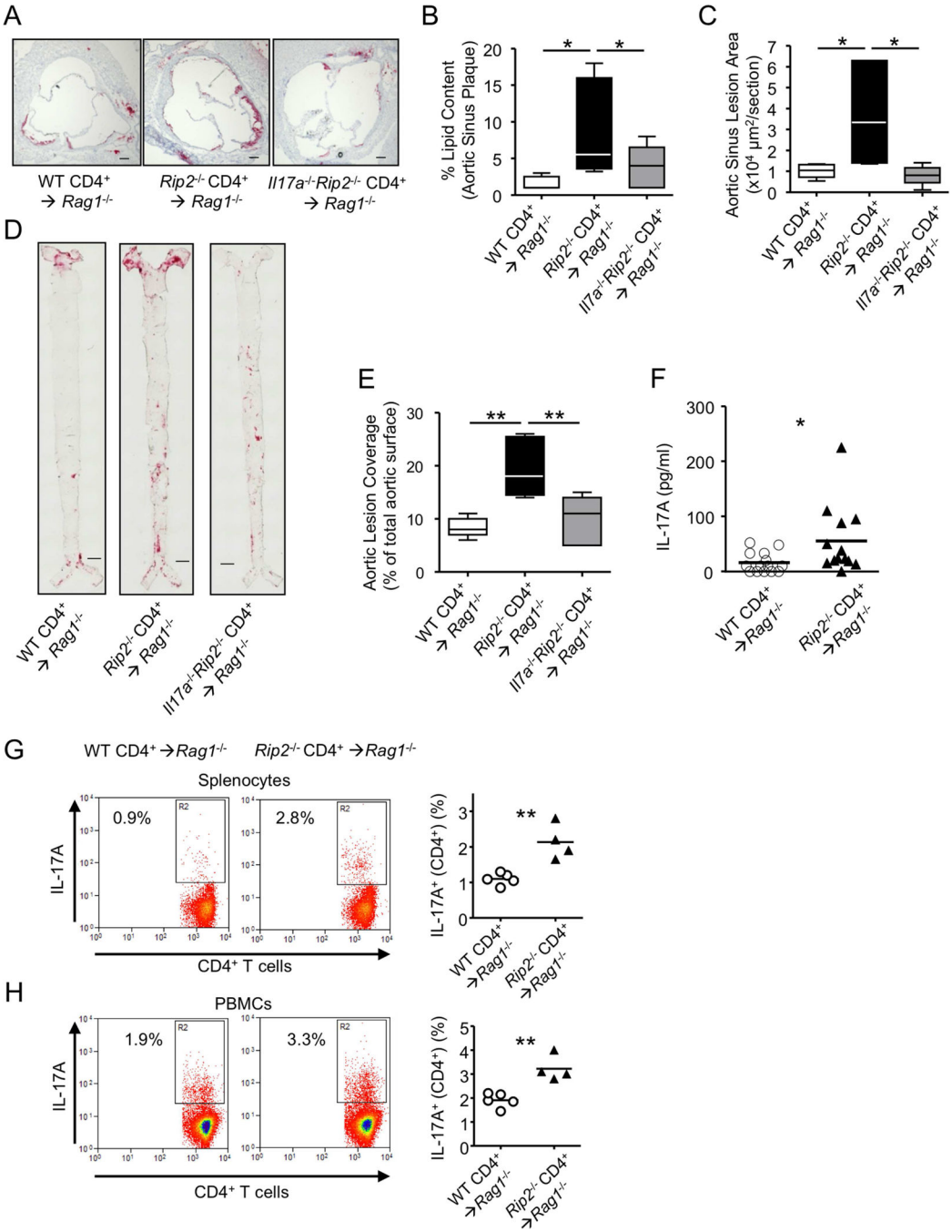

Figure 4. RIP2 deficiency enhances IL-17A dependent atherogenesis.

WT, *Rip2*$^{-/-}$, *and Il17a*$^{-/-}$*Rip2*$^{-/-}$ naïve CD4^{+} T cells were adoptively transferred to *Rag1*$^{-/-}$ mice. Mice were infected with AAV-PCSK9 and fed a HFD for 12 weeks. (A) Oil red O staining of aortic sinus. Scale bars represent 200 µm. (B) Lipid content within the aortic sinus. (C) Aortic sinus lesion area. (D) Oil red O staining of aorta en face. Scale bars represent 1 mm. (E) Aorta en face lesion coverage. Data are representative of two independent experiments combined (n=13 mice/group). (F) IL-17A concentration in plasma (n=14–15 mice/group). (G and H) Flow cytometry plots and graphs of IL-17A expressing

$CD4^+$ T cells in splenocytes (G) and PBMCs (H). Data are representative of two independent experiments (n=4–5 mice/group). Statistical analyses: one-way ANOVA followed by Tukey's post-hoc test (B, C and E) or Student's *t*-test (F-H). $*$ $p < 0.05$, $**$ $p < 0.01$. See also Figure S4.

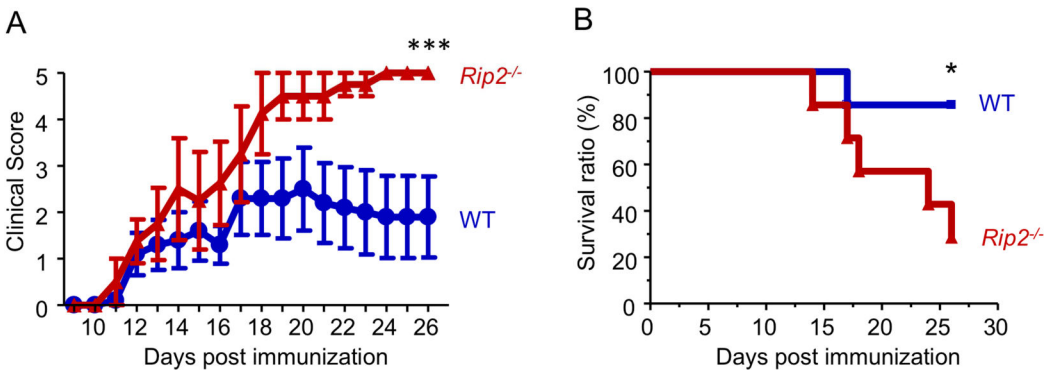

Figure 5: RIP2 deficiency in CD4$^+$ T cells enhances severity and mortality of EAE.

WT and *Rip2*$^{-/-}$ CD4$^+$ T cells were adoptively transferred to *Rag1*$^{-/-}$ mice. EAE was induced with MOG35–55 and PTx. (A) EAE clinical score. Data are representative of two independent experiments (n=4–5). (B) Percent survival. Data are representative of two independent experiments combined (n=7). Statistical analyses: two-way ANOVA (A) or chi-square test (B). $*$ $p < 0.05$, $***$ $p < 0.001$. Results are represented as mean ± SEM.

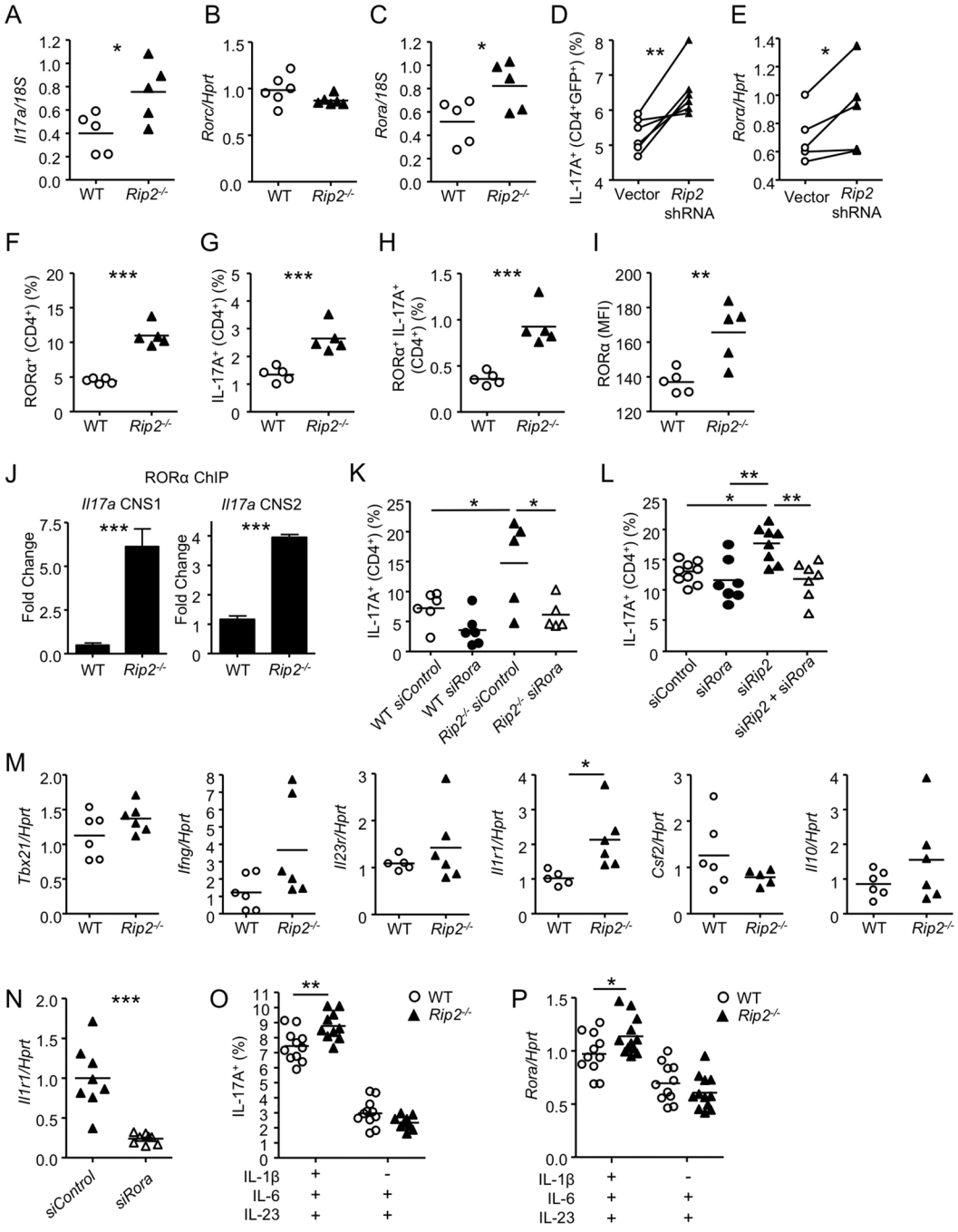

Figure 6: RORα and IL-1β mediate the enhanced pathogenic Th17 cell differentiation of RIP2 deficient T cells.

Naïve CD4$^+$ T cells were isolated from the spleens of WT and *Rip2*$^{-/-}$ mice and differentiated *in vitro* with anti-CD3 and anti-CD28 Ab in the presence of pTh17 cell differentiation cytokines. (A-C) qPCR of *Il17a* (A), *Rora* (B) and *Rorc* (C) mRNA expression from pTh17 cells (n=5–6). (D) Flow cytometry analysis of IL-17A expression in *in vitro* derived pTh17 cells differentiated following transduction with control or *Rip2* shRNA retrovirus (n=6). (E) qPCR of *Rora* mRNA expression in *in vitro* derived pTh17 cells differentiated following transduction with control or *Rip2* shRNA retrovirus (n=5). (F-

I) Percent of *in vitro* derived pTh17 cells expressing RORα (F) and IL-17A (G). Percent of *in vitro* derived pTh17 cells expressing IL-17A and RORα (H). MFI of RORα expression in IL-17A^{+} pTh17 cells (I) (n=5). (J) RORα binding to CNS1 and CNS2 in the *Il17a* locus as measured by ChIP with anti-RORα antibody followed by qPCR (n=5). (K) IL-17A expression in *in vitro* derived WT and *Rip2*$^{-/-}$ pTh17 cells differentiated in the presence of control siRNA or siRNA targeting *Rora* (n=5–6). (L) IL-17A expression in *in vitro* derived pTh17 cells differentiated in the presence of control siRNA or siRNA targeting *Rora* and/or *Rip2* (n=7–9). (M) qPCR of *Tbx21*, *Ifng*, *Il23r*, *Il1r1*, *Csf2* and *Il10* expression in pTh17 cells (n=5). (N) qPCR or *Il1r1* expression in *Rip2*$^{-/-}$ pTh17 cells differentiated in the presence of control siRNA or siRNA targeting *Rora* (n=8). (O) IL-17A expression in *in vitro* derived Th17 cells differentiated in the presence of indicated cytokines (n=10–11). (P) qPCR of *Rora* expression in *in vitro* derived Th17 cells differentiated in the presence of indicated cytokines (n=11–12). Data are representative of two to three independent experiments (A-L, N-P) or one independent experiment (M). Statistical analyses: Student's *t*-test (A-B, E-J, M, N-P), paired Student's *t*-test (D-E) or one-way ANOVA followed by Tukey's post-hoc test (K-L). $*$ $p < 0.05$, $**$ $p < 0.01$, $***$ $p < 0.001$. See also Figure S5.

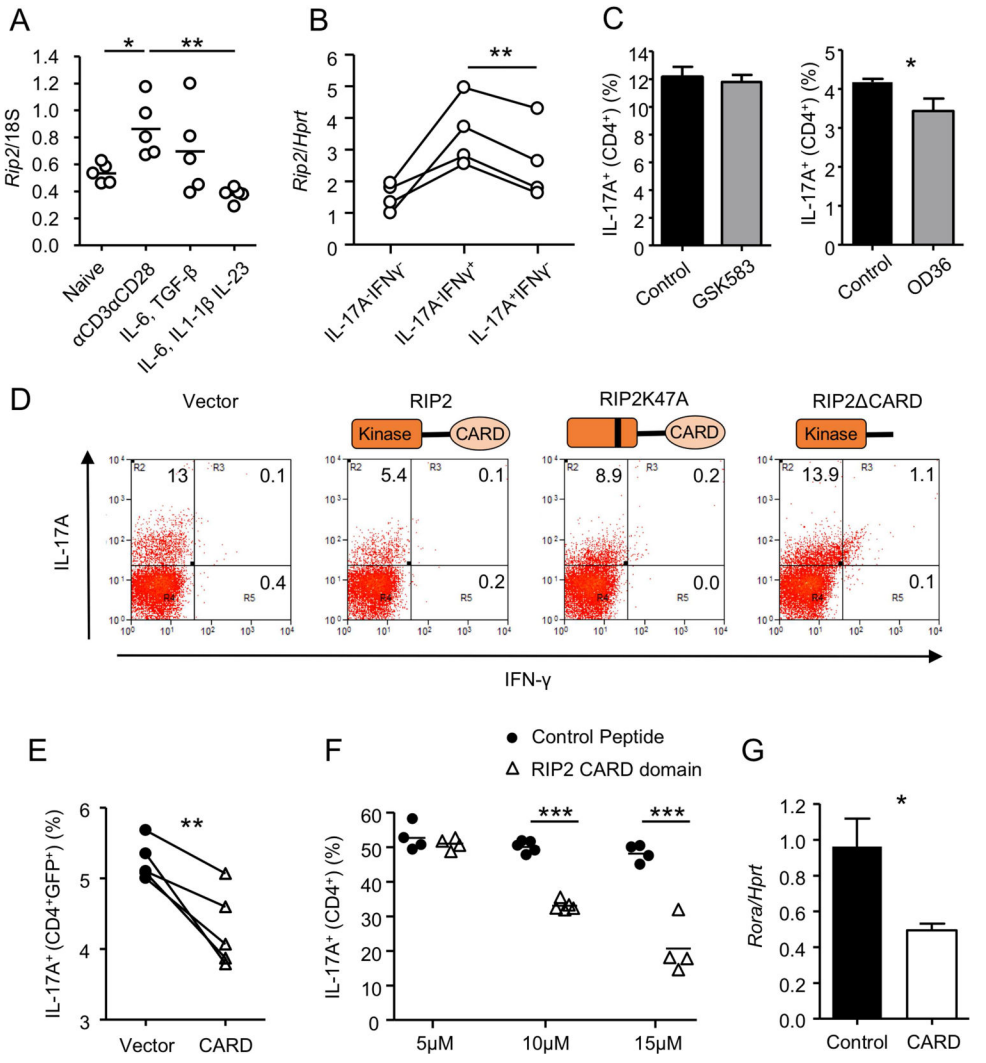

Figure 7: RIP2 CARD domain suppresses pathogenic Th17 cell differentiation.

(A) qPCR of *Rip2* expression in splenic naïve CD4$^+$ T cells differentiated *in vitro* with anti-CD3 and anti-CD28 Ab alone or in the presence of cTh17 cell or pTh17 cell differentiation cytokines. (B) qPCR of *Rip2* expression in flow cytometry sorted IL-17A$^-$IFN-γ$^-$, IL-17A$^-$IFN-γ$^+$ and IL-17A$^+$IFN-γ$^-$ cells from IL-17A and IFN-γ reporter mice infected intratracheally with *C. pneumoniae* (1×10^6 IFU) for 21 days. (C) IL-17A expression in *in vitro* derived pTh17 cells treated with RIP2 kinase inhibitors GSK583 or OD36. (D) IL-17A and IFN-γ expression in *in vitro* derived pTh17 cells following transduction with control, RIP2, RIP2K47A or RIP2ΔCARD retrovirus. (E) Percent of IL-17A inhibition in *in vitro* derived pTh17 cells following transduction with control or RIP2 CARD domain (RCD) retrovirus. (F) Percent of IL-17A expression in *in vitro* derived pTh17 cells treated with indicated concentrations of cell penetrating peptides; dNP2-FLAG (control) or dNP2-FLAG-CARD (RCD). (G) qPCR of *Rora* expression in *in vitro* derived pTh17 cells treated with dNP2-FLAG (control) or dNP2-FLAG-CARD (RCD) peptides. Data are representative of two to three independent experiments (A-D, F-G) or one independent experiment (E) (n=4–5). Statistical analyses: one-way ANOVA followed by Tukey's post-hoc test (A), Student's *t*-

test (C, F-G) or paired Student's *t*-test (B and E). * $p < 0.05$, ** $p < 0.01$, *** $p < 0.001$. See also Figure S6.